Title: ETV7 limits antiviral gene expression and control of SARS-CoV-2 and influenza viruses

Authors: Heather M. Froggatt[1], Alfred T. Harding[1], Brook E. Heaton[1], and Nicholas S. Heaton[1,*]

[1]Department of Molecular Genetics and Microbiology
Duke University School of Medicine
Durham, NC 27710, USA

*To whom correspondence should be addressed:
Nicholas S. Heaton, PhD
Assistant Professor
Department of Molecular Genetics and Microbiology (MGM)
Duke University Medical Center
213 Research Drive, 426 CARL Building, Box 3054
Durham, NC 27710
Tel: 919-684-1351
Fax: 919-684-2790
Email: nicholas.heaton@duke.edu

One Sentence Summary: ETV7 is an interferon-induced, repressive transcription factor that negatively regulates antiviral interferon-stimulated genes essential for controlling influenza virus and SARS-CoV-2 infections.

Abstract

The type I interferon (IFN) response is an important component of the innate immune response to viral infection. Precise control of interferon responses is critical; insufficient levels of interferon-stimulated genes (ISGs) can lead to a failure to restrict viral spread while excessive ISG activation can result in interferon-related pathologies. While both positive and negative regulatory factors control the magnitude and duration of IFN signaling, it is also appreciated that a number of ISGs regulate aspects of the interferon response themselves. However, the mechanisms underlying these ISG regulatory networks remain incompletely defined. In this study, we performed a CRISPR activation screen to identify new regulators of the type I IFN response. We identified ETS variant transcription factor 7 (ETV7), a strongly induced ISG, as a protein that acts as a negative regulator of the type I IFN response; however, ETV7 did not uniformly suppress ISG transcription. Instead, ETV7 preferentially targeted a subset of known antiviral ISGs. Further, we showed the subset of ETV7-modulated ISGs was particularly important for IFN-mediated control of some viruses including influenza viruses and SARS-CoV-2. Together, our data assign a function for ETV7 as an IFN response regulator and also identify ETV7 as a therapeutic target to increase innate responses and potentiate the efficacy of interferon-based antiviral therapies.

18 **Introduction**

19 The type I interferon (IFN) response is a transient innate immune defense system that, upon
20 activation by viral infection or therapeutic IFN treatment, induces the transcription of hundreds of
21 interferon-stimulated genes (ISGs) (*1*). Many ISGs have characterized antiviral roles that restrict
22 viral replication by either interfering with viral processes directly or altering cellular pathways
23 required for viral replication (*2*). However, because replication mechanisms and points of
24 interaction with the cell differ between viruses, individual ISGs have varying potencies against
25 different viruses (*3–5*). As a result, unique combinations of ISGs are thought to mediate successful
26 antiviral responses against distinct viruses (*1*, *6*).

27

28 The canonical activation pathway of the type I IFN signaling pathway induced by viral infection,
29 or after therapeutic administration (*7*), is well understood (*8*, *9*). Extracellular IFN is bound by its
30 cognate plasma membrane-localized receptor (IFNAR1/2). Downstream effectors (JAK proteins)
31 are phosphorylated to then activate formation of the interferon-stimulated gene factor 3 (ISGF3)
32 complex. Finally, the ISGF3 complex of STAT1, STAT2, and IRF9 translocates to the nucleus (*8*)
33 and binds the interferon sensitive response element (ISRE), with the consensus DNA motif
34 GAAANNGAAA, to activate transcription of ISGs (*10*).

35

36 As infection is cleared and virally-derived innate immune activators become scarce, interferon
37 production is reduced and the interferon-stimulated gene response is downregulated. To facilitate
38 this return to cell homeostasis, IFN induced negative regulators, such as SOCS1 (*11*) and USP18
39 (*12*), act at multiple levels in the signaling pathway (*13*). Thus, negative regulators of IFN
40 responses are an important group of IFN-stimulated genes that control the duration of ISG
41 induction and activity. Antagonism of interferon response negative regulators has been proposed
42 as a mechanism to enhance host antiviral responses to clear infection, both alone and in conjunction

43 with IFN treatment (*14–16*), and most recently during the COVID-19 pandemic (*17*). However,
44 regulators working upstream of transcription impact ISGs indiscriminately, including suppression
45 of the pro-inflammatory effectors, that when overabundant, can induce a cytokine storm; for
46 example, agonists of an IFNAR-downregulating protein, S1PR1 (*18*), are proposed for use against
47 pandemic influenza viruses (*19*) and SARS-CoV-2 (*20*) to instead limit excessive immune
48 responses associated with interferon signaling. An ideal negative regulator of the IFN response for
49 antiviral therapeutic targeting would enhance virus restricting ISGs specifically, without affecting
50 pro-immune cytokines.
51
52 In addition to the upstream regulators that broadly activate or suppress IFN responses, there are
53 interferon-induced transcriptional regulators that enhance, limit, or fine-tune ISG activity (*21*).
54 Many ISGs themselves participate in innate immune signaling to amplify IFN and other pro-
55 immune responses (*22*). Activators also add complexity by inducing non-canonical IFN response
56 pathways or specific groups of ISGs. Interferon responsive factors (IRFs) 1 and 7 are ISGs and
57 transcription factors that activate subsets of ISGs (*23*, *24*). Further, recent work has shown that
58 ELF1 (E74-like ETS transcription factor) is induced by IFN and facilitates the expression of a
59 group of genes not otherwise activated by the IFN response (*25*). Additional regulatory steps for
60 ISGs, post-JAK/STAT signaling, likely exist to allow the cell to fine-tune its antiviral activity for
61 an effective and appropriate response. While interferon-induced positive regulators of the IFN
62 response are known to shape the complexity of ISG activation, reports of analogous roles for
63 negative regulators remain conspicuously absent.
64
65 To address this gap in knowledge and identify genes able to shape the IFN response through
66 negative regulation, we performed a CRISPR activation (CRISPRa) screen that selected for factors
67 sufficient to prevent expression of an ISRE-containing IFN response reporter. We identified ETV7

68 (ETS variant transcription factor 7) as a negative regulator of the type I IFN response with a role
69 in controlling the expression of specific ISGs. We further showed the ETV7-modulated ISGs are
70 important for control of some IFN-sensitive respiratory viruses. Together, these data demonstrate
71 ETV7 is a suppressive component of the complex ISG regulatory network that could be targeted
72 to enhance specific antiviral responses against influenza viruses and SARS-CoV-2 (*1*, *26*).
73
74 **Results**
75 *A CRISPR activation screen identifies ETV7 as a negative regulator of the type I IFN response.*
76 In order to identify negative regulators of the type I IFN response, we developed a type I IFN
77 response reporter that included seven copies of the consensus interferon sensitive response element
78 (ISRE) ahead of a minimal CMV promoter controlling expression of sfGFP (**Fig. 1A**). To make
79 our reporter temporally specific, sfGFP was fused to a mouse ornithine decarboxylase (MODC)
80 protein degradation domain to decrease its half-life (*27*). We stably introduced this construct into
81 the A549 lung epithelial cell line along with a dCAS9-VP64 fusion protein and a MS2-p65-HSF1
82 activator complex required for the SAM CRISPR activation (CRISPRa) system (*28*). After clonal
83 selection, 99.8% of the A549-SAM-IFN response cells expressed GFP in response to type I IFN
84 treatment (**Fig. 1B and C**).
85
86 To perform the screen, we took the A549-SAM-IFN response cell line and introduced a lentivirus
87 library containing sgRNAs designed to activate every putative ORF in the human genome (*28*)
88 (**Fig. 1D**). After 48 hours, half of the cells were collected to determine the transduction efficiency
89 and the remaining cells were re-plated for IFN stimulation. At 72 hours post-sgRNA introduction,
90 the cells were treated with IFN-α and collected for fluorescence-activated cell sorting (FACS).
91 During sorting, we eliminated reporter-positive cells and collected only cells that were
92 nonresponsive to IFN as this population should theoretically be overexpressing a negative

Figure 1

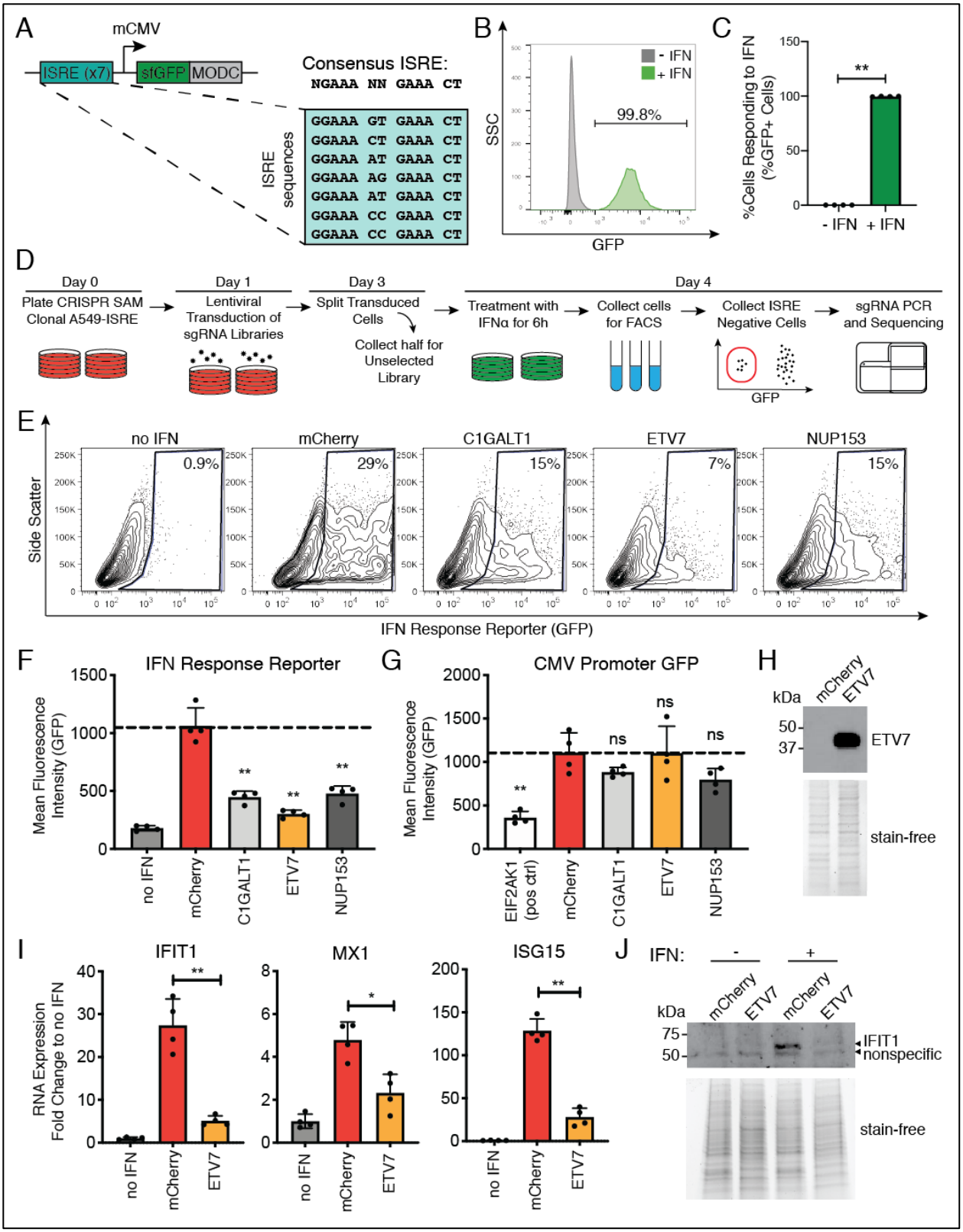

Fig. 1. A CRISPR activation screen identifies ETV7 as a negative regulator of the type I interferon response. (**A**) Diagram of the IFN response reporter used to identify cells responding to IFN. ISRE = interferon sensitive response element, MODC = protein degradation domain. (**B**) Flow cytometry histogram and (**C**) bar graph of A549-SAM-IFN response cells before and after IFN-α treatment (1000 U/mL, 6 h) (data shown as mean ± SD, n=4, statistical analysis relative to

Fig. 1. (continued) untreated control). (**D**) Diagram of CRISPRa screen workflow to identify negative regulators of the type I IFN response. (**E**) Flow cytometry plots of 293T cells transfected with the IFN response reporter and overexpression plasmids for the indicated screen hits and then treated with IFN-α (100 U/mL, 9 h). (**F**) Quantification of **E** showing brightness of cells expressing GFP compared to the mCherry-expressing control (data shown as mean ± SD, n=4). (**G**) Brightness of cells expressing GFP from a constitutively expressing plasmid in cells overexpressing the indicated genes (positive control = EIF2AK1/HRI, shuts off translation) compared to control (data shown as mean ± SD, n=4). (**H**) Western blot showing ETV7 protein levels in 293T cells transfected with the ETV7 overexpression plasmid. Stain-free gel imaging was used to confirm equal loading. (**I**) Endogenous ISG mRNA expression levels measured using RT-qPCR after IFN-α treatment (100 U/mL, 9 h) (data shown as mean ± SD, n=4). (**J**) Western blot comparing IFIT1 protein levels in control and ETV7 overexpressing cells after IFN-α treatment (500 U/mL, 18 h). Stain-free gel imaging was used to confirm equal loading. For all panels: P-values calculated using unpaired, two-tailed Student's t-tests (*$p<0.05$, **$p<0.001$) compared to mCherry-expressing control samples unless otherwise noted.

94 regulator of the IFN response. We performed two independent biological replicates of the screen
95 and sequenced the sgRNA-containing amplicons derived from our input DNA, unselected
96 transduced cells, and cells that were nonresponsive to type I IFN. Raw sequencing data was
97 aligned, mapped, and subsequently analyzed using the MAGeCK pipeline (*29*) to generate z-score
98 values for each gene. Genes were defined as "hits" if their z-scores exceeded two standard
99 deviations from the mean, resulting in an overlap of 10 high-confidence genes between the two
100 screen replicates (**Fig. S1A, Table S1, Data files S1 and S2**). We were seeking to identify
101 regulators of the IFN response that are regulated by IFN themselves; therefore, we selected hits
102 for validation previously reported to have at least a two-fold induction after IFN stimulation in the
103 Interferome database (*30*). This analysis identified three hits (C1GALT1, ETV7, and NUP153) as
104 potential negative regulators of the type I IFN response (**Table S1**).
105
106 To validate our three hits, and to eliminate any potential off-target effects of CRISPRa, we cloned
107 the three ORFs and validated overexpression of the genes in 293T cells (**Fig. S1B**). Co-transfection
108 of the overexpression plasmids and IFN response plasmid, followed by stimulation with IFN-α,
109 resulted in lower reporter expression compared to a control mCherry-expressing plasmid (**Fig. 1E**

110 **and F, Fig. S1C**). To verify this repressive activity was specific to the IFN response and the hits
111 were not general inhibitors of transcription or translation, we transfected the overexpression
112 plasmids along with a constitutively active GFP-expressing plasmid. We included a positive
113 control (EIF2AK1/HRI), which is known to suppress host translation when overexpressed (*31*).
114 None of the potential hits significantly reduced expression of the GFP-expressing plasmid (**Fig.**
115 **1G, Fig. S1D**). We therefore chose ETV7 for further characterization because: 1) NUP153 has
116 previously been shown to control the distribution of STAT1 in the cell (*32*), 2) ETV7 had not been
117 reported to play a role in the IFN response, and 3) it had the strongest inhibitory phenotype against
118 the IFN response reporter.
119
120 After confirming overexpression of ETV7 at the protein level (**Fig. 1H**), we verified that the
121 inhibitory effects of ETV7 were not restricted to the IFN response reporter plasmid. We collected
122 mRNA and protein from IFN-α stimulated ETV7 overexpression cells to quantify effects on the
123 expression of endogenous ISGs. ETV7 overexpression significantly repressed the induction of
124 three prototypical ISGs (IFIT1, MX1, and ISG15) at the RNA level (**Fig. 1I**). The reduction of
125 ISG expression during ETV7 overexpression was also demonstrated at the protein level for IFIT1
126 (**Fig. 1J**). These data together demonstrate that overexpression of ETV7 alone is sufficient to
127 repress ISG induction by type I IFN.
128
129 *ETV7 acts as a transcription factor to repress IFN-induced expression.*
130 ETV7 is known to be a repressive transcription factor (*33*, *34*), although a role in repressing type
131 I IFN responses has never been reported. To determine whether ETV7 acts as a transcription factor
132 in this context, we generated a previously validated mutant of ETV7, called ETV7(KALK), which
133 is unable to bind DNA (**Fig. 2A and B**) (*35*). Overexpression of ETV7(KALK) and stimulation

Figure 2

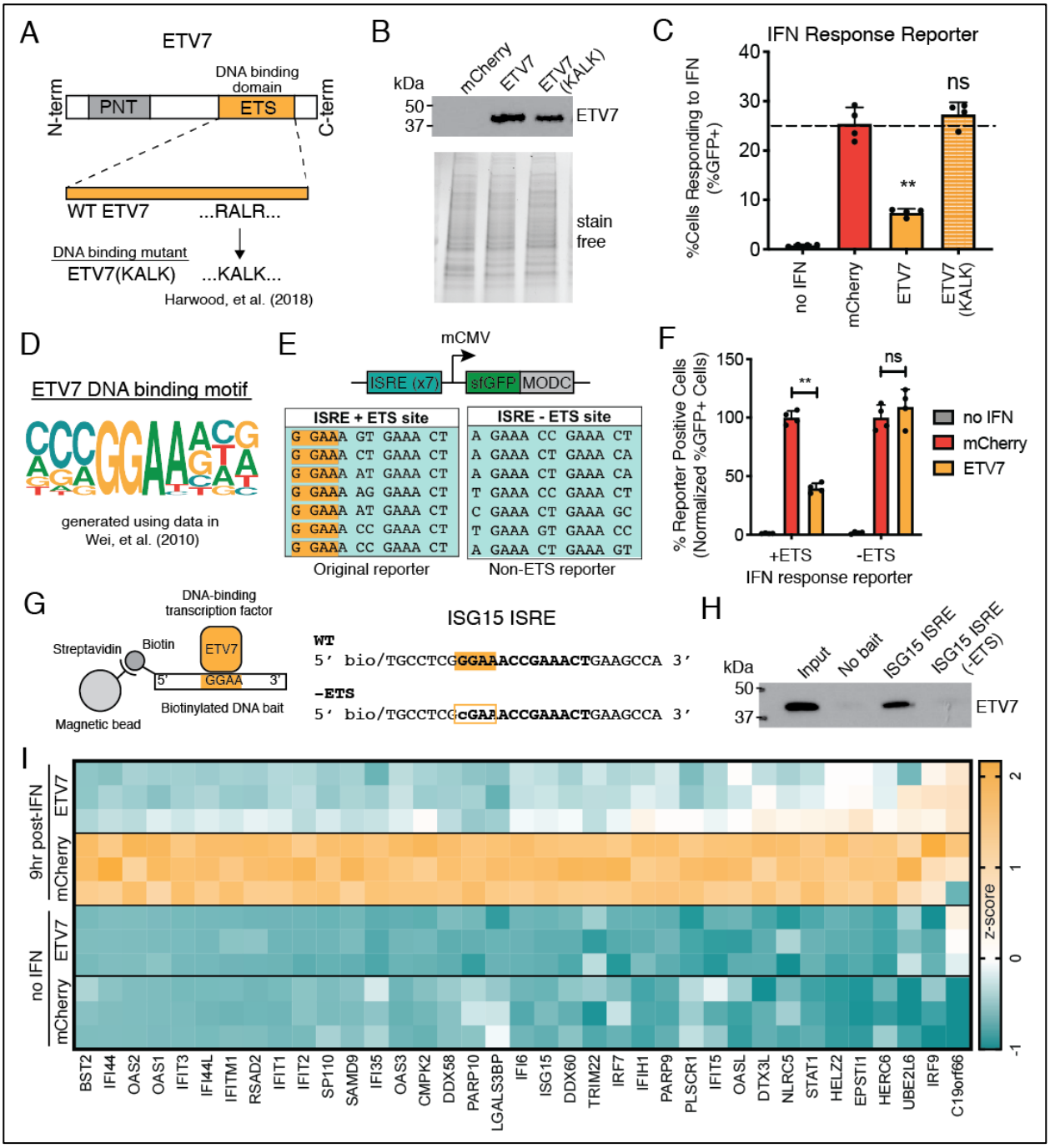

134

Fig. 2. ETV7 acts as a transcription factor to negatively regulate the type I IFN response. (**A**) Diagram showing the ETV7 protein domains and amino acid changes made to generate the DNA binding mutant, ETV7(KALK). (**B**) Western blot showing ETV7 protein levels in 293T cells transfected with WT or DNA binding mutant (KALK) ETV7 expression plasmids. Stain-free gel imaging was used to confirm equal loading. (**C**) Percent of 293T cells expressing GFP from the IFN response reporter with overexpression of WT or DNA binding mutant (KALK) ETV7 after IFN-α treatment (100 U/mL, 9 h) compared to control (data shown as mean ± SD, n=4). (**D**) ETV7's DNA binding position weighted matrix (PWM) generated using enoLOGOS (*99*) with data from Wei et al. (*36*). (**E**) Diagrams of the IFN response reporters containing (+ETS) and not containing (-ETS) potential ETV7 binding sites (ETS site, highlighted in yellow). (**F**) Normalized percent of 293T cells expressing GFP from IFN response reporters either containing or not

Fig. 2. (continued) containing ETS sites after overexpression of ETV7 and IFN-α treatment (100 U/mL, 6 h) compared to mCherry-expressing control (data shown as mean ± SD, n=4). (**G**) Diagram of the DNA pull-down experiment using biotinylated DNA and streptavidin-coated magnetic beads to show binding of a transcription factor to a specific DNA sequence. Sequences of biotinylated DNA bait used to show binding of ETV7 to the WT ISG15 ISRE (*93*) and loss of binding with mutation of the ETS binding site (-ETS). (**H**) Western blot of DNA pull-down using biotinylated oligos containing the ISG15 ISRE sequence in its wild-type form (WT) or with a single nucleotide mutation (-ETS) to eliminate the ETS site, incubated with nuclear lysate from cells expressing ETV7 with IFN treatment (100 U/ml, 9 h). (**I**) Heat map displaying RNA levels of genes upregulated at least 2.5-fold following IFN-α treatment (100 U/mL, 9 h) in control (mCherry) cells. Yellow = upregulated, blue = downregulated. For all panels: P-values calculated using unpaired, two-tailed Student's t-tests (*p<0.05, **p<0.001) relative to IFN-stimulated, mCherry-expressing control samples.

135 with IFN-α had no measurable effect on expression of the IFN response reporter, in contrast to
136 WT ETV7 overexpression (**Fig. 2C, Fig. S2A**).
137
138 ETV7 has been reported to bind the canonical ETS family DNA motif, GGAA (*36*), known as an
139 "ETS" site (**Fig. 2D**). The original IFN response reporter design contained multiple ETS sites (**Fig.**
140 **2E**), which likely explains why it is negatively impacted by ETV7 in our screen. To test the
141 requirement of ETS sites for ETV7 repressive activity against our reporter, we generated an IFN
142 response reporter containing seven consensus ISREs from canonical ISGs that all lack ETS sites
143 (ISRE -ETS) (**Fig. 2E**). We transfected the two reporter plasmids (ISRE +ETS and ISRE -ETS)
144 independently into 293T cells and stimulated with IFN-α. As expected, both reporter plasmids
145 responded to IFN treatment and were repressed by overexpression of known negative regulators
146 of the type I IFN response (SOCS1, USP18) that function upstream of transcription (**Fig. S2B**).
147 When ETV7 was transfected into cells with the IFN response reporters and stimulated with IFN
148 however, the repressive activity of ETV7 was restricted to the reporter plasmid containing ETS
149 motifs (**Fig. 2F, Fig. S2C**).
150

151 To provide evidence of ETV7 directly binding ISRE motifs containing ETS sites, we performed a
152 DNA oligo-based pull-down experiment using the ISG15 ISRE sequence (**Fig. 2G**). We chose this
153 ISRE because 1) it contains an ETS binding site, 2) it was included in our initial IFN response
154 reporter, and 3) ETV7 was shown to impact ISG15 induction (**Fig. 1I**). In addition to the wild-
155 type ISG15 ISRE biotinylated oligos, we tested biotinylated oligos with a single nucleotide
156 mutation that eliminates the ETS site in the ISG15 ISRE (-ETS). We generated nuclear lysates
157 from 293T cells overexpressing ETV7 and treated with IFN-α, incubated the lysate with either the
158 biotinylated WT or -ETS ISG15 ISRE oligos, and pulled down the biotinylated DNA using
159 streptavidin-coated magnetic beads. Western blotting for ETV7 protein revealed the transcription
160 factor bound the WT ISG15 ISRE containing the ETS site, but not the mutated version of the
161 promoter lacking the ETS site (**Fig. 2H**). Together, these experiments demonstrate that the
162 repressive activity of ETV7 requires both its ability to bind DNA and the presence of ETS sites in
163 the target ISG promoters.
164
165 *ETV7 non-uniformly represses IFN-stimulated gene expression*
166 Since consensus ISREs can either contain or lack a GGAA motif (**Table S2**), we hypothesized
167 ETV7 could differentially act on specific ISGs based on the presence or absence of ETS sites in
168 their ISRE sequences and promoters. To perform an unbiased examination of the effect of ETV7
169 upregulation, we performed RNA sequencing in cells with or without ETV7 overexpression and
170 IFN stimulation (**Data file S3 and Fig. S2E).** To identify the types of genes, processes, and
171 functions impacted by overexpression of ETV7, we generated lists of the most downregulated
172 genes during ETV7 overexpression, both before and after IFN treatment, and performed gene set
173 enrichment analyses. This analysis technique takes a gene list and returns overrepresented terms
174 from gene and protein databases (*37*). In the absence of IFN treatment, the most significantly
175 enriched terms were not biological pathways, but rather ETS family transcription factor binding

176 motifs (**Table S3**); this is expected, as ETV7 is an ETS family member and the entire family binds
177 the same core motif, GGAA. In contrast, the genes specifically downregulated by ETV7 during
178 IFN treatment were highly enriched for processes and pathways associated with responses to
179 interferon and viral infection (**Table S4**). To visualize the effect of ETV7 upregulation specifically
180 on ISGs, we generated a heat map of the genes induced at least 2.5-fold upon IFN treatment in our
181 RNA sequencing experiment (**Fig. 2I**). Consistent with our hypothesis, we found some genes were
182 suppressed by ETV7 overexpression more than others (**Fig. 2I**).
183
184 Although we had previously immunoprecipitated ETV7 with ISRE-containing oligos (**Fig. 2H**),
185 we next wanted to demonstrate ETV7 occupancy on native ISG promoters for genes targeted by
186 ETV7 via chromatin immune-precipitation followed by quantitative PCR (ChIP-qPCR). To enable
187 these experiments, we first generated a FLAG-tagged ETV7 (**Fig. S2E**) and demonstrated that the
188 tag does not disrupt its ability to repress the IFN response reporter (**Fig. S2F**). We next selected
189 the promoter of IFI44L for ChIP analysis as it was both highly affected by ETV7 and also harbors
190 many ETS sites within ISRE-like sequences in its promoter (**Fig. 2I and Fig. S2G and H**). To
191 perform ChIP-qPCR, we generated sheared chromatin after cross-linking cells transfected with
192 FLAG-tagged ETV7 and treated with IFN-α. We then performed immunoprecipitation using either
193 nonspecific IgG or anti-FLAG antibodies raised in mice or rabbits. After qPCR analysis, we found
194 no enrichment for a negative control region (the gene desert on chromosome 12) between the IgG
195 and anti-FLAG samples (**Fig. S2I**). In contrast, DNA corresponding to the IFI44L promoter was
196 significantly enriched with both the rabbit and mouse anti-FLAG samples compared to the
197 nonspecific IgG samples (**Fig. S2I**). These experiments demonstrate that ETV7 acts as a
198 transcription factor to bind and suppress ISG promoters that containing GGAA motifs.
199
200

201 *ETV7 loss enhances antiviral IFN-stimulated gene expression.*

202 Our experiments up to this point had primarily utilized overexpression of ETV7. One major
203 disadvantage of this approach is the non-physiological kinetics and magnitude of ETV7 expression
204 relative to what is observed after IFN stimulation in cells (**Fig. 3A**). To define the physiological
205 effects of ETV7 induction during the IFN response, we performed a series of loss-of-function
206 experiments. Our expectation was that the knockout of ETV7 would have the reciprocal effect on
207 IFN responses as protein overexpression (*38*). We transduced A549-IFN response reporter cells
208 (the original reporter with ISRE +ETS sites) with Cas9 and separately, two independent sgRNAs
209 targeting ETV7, KO1(sg16667) and KO2(sg16668), generated pooled lines using antibiotic
210 selection, and then stimulated with IFN-α. Both guides resulted in significantly more IFN-induced
211 sfGFP expression compared to a control sgRNA (**Fig. 3B, Fig. S3A**).

212

213 We next generated clonal ETV7 knockout A549 lung epithelial cell lines (KO1-1, KO1-2) lacking
214 the reporter and sequenced the resulting DNA lesions to confirm ETV7 knockout. Since ETV7 is
215 normally only expressed after IFN stimulation, we treated with IFN-α and verified a reduction in
216 ETV7 expression at the RNA level, presumably via nonsense mediated RNA decay (**Fig. 3C**). A
217 representative housekeeping gene (ACTB) displayed no significant increases in transcription in
218 any of the ETV7 KO clones (**Fig. 3D**). We then selected twelve ISGs (IFITM1, RSAD2, OAS1-
219 3, IFIT1-3, IFI44L, ISG15, BST2, and IFI44) that were highly impacted by ETV7 in our RNA
220 sequencing results for RT-qPCR analysis after IFN treatment. Compared to clonal lines containing
221 a non-targeting guide, the ETV7 KO lines showed significant increases in induction of each of the
222 twelve ISGs (**Fig. 3E-K, Fig. S3B-F**). Thus, the physiological induction of ETV7 after IFN
223 stimulation affects the expression of ISGs.

224

225

Figure 3

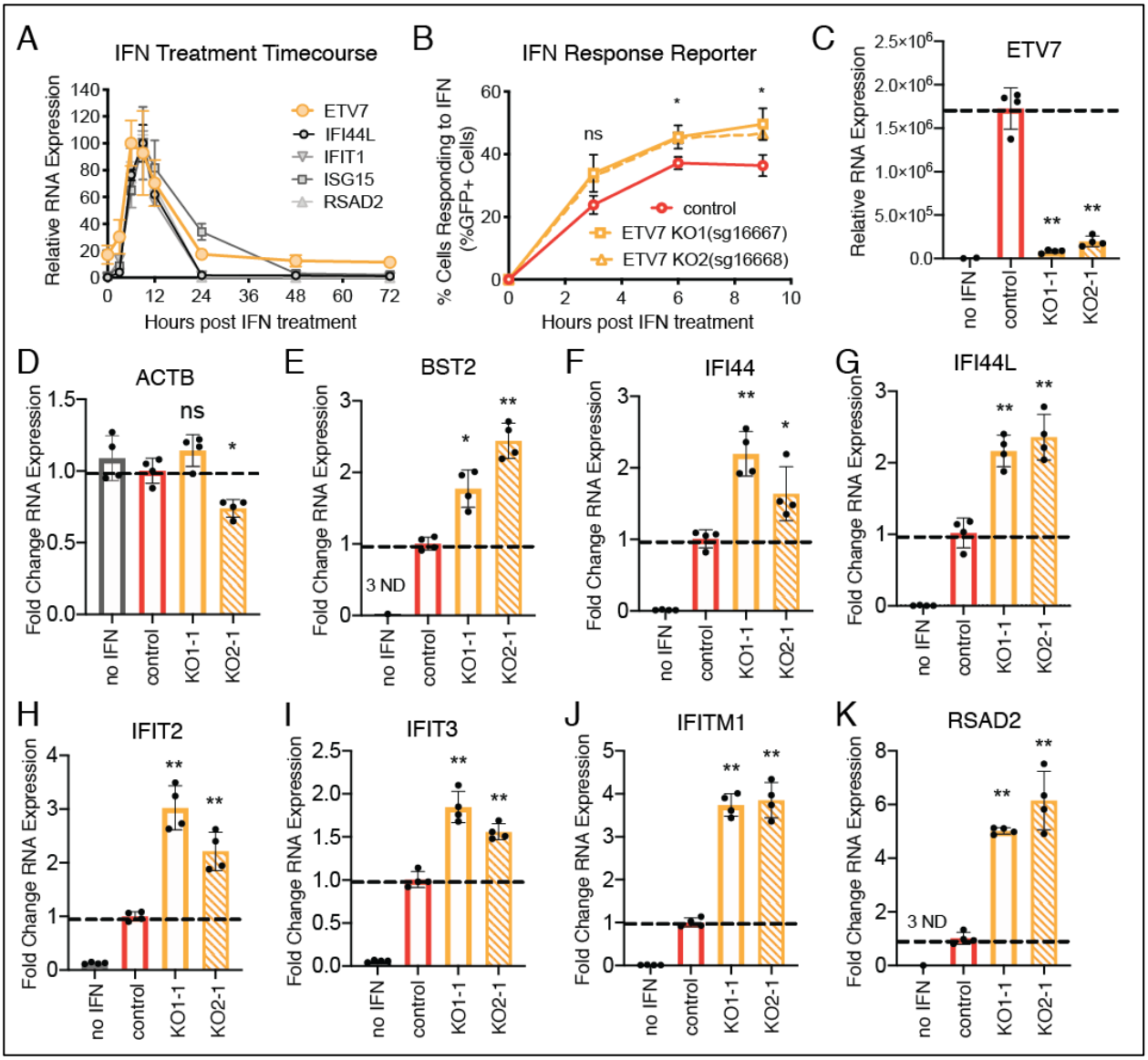

226

Fig. 3. Loss of ETV7 enhances expression of ISGs. (**A**) ETV7 and other ISG mRNA levels in A549 lung epithelial cells after IFN-α treatment (100 U/mL, 6 h) (data shown as mean ± SD, n=4). (**B**) Percentage of cells expressing GFP from the IFN response reporter in two A549 ETV7 KO cell lines (pooled, 2 different guides) after IFN-α treatment (1000 U/mL, 6 h) compared to non-targeting control cells (data shown as mean ± SD, n=3). (**C**) mRNA levels of ETV7 in non-targeting control and ETV7 KO A549 clonal cell lines after IFN-α treatment (1000 U/mL, 6 h) (data shown as mean ± SD, n=4). (**D-K**) mRNA levels of a housekeeping gene (**D**) and ISGs (**E-*K***) in control and ETV7 KO A549 clonal cell lines after IFN-α treatment (100 U/mL, 9 h) (data shown as mean ± SD, n=4). For all panels: P-values calculated using unpaired, two-tailed Student's t-tests (*p<0.05, **p<0.001) compared to IFN-stimulated, non-targeting sgRNA control samples.

227 *Suppression of ETV7 enhances IFN-mediated control of influenza viruses and SARS-CoV-2.*

228 In trying to predict the physiological significance of excessive induction of these ETV7-regulated

229 ISGs during the type I IFN response, we noted that many have recognized antiviral functions (*2*,

230 *39*, *40*). To determine whether the effects of ETV7 suppression of ISG expression were relevant
231 in the context of a viral infection, we wanted to identify a virus restricted by the ISGs most affected
232 by ETV7 (*41*). Many of these genes with well-recognized antiviral functions (IFITM1, IFIT1-3,
233 OAS1-3, BST2, RSAD2) have been reported to play important roles in the restriction of influenza
234 viruses (*42*). IFITM1 has been shown to prevent viral entry (*43*), OAS proteins activate RNase L
235 to degrade viral RNA (*44*), IFITs bind viral RNA and promote antiviral signaling (*45*), and
236 BST2/Tetherin and RSAD2/Viperin restrict viral budding and egress (*46*, *47*). Therefore, we
237 hypothesized that ETV7 dysregulation would affect influenza virus replication and spread.
238
239 We first infected our ETV7 KO A549 cells with a laboratory-adapted H1N1 influenza A virus
240 (IAV), A/Puerto Rico/8/1934 (PR8). Using a hemagglutination (HA) assay to measure the number
241 of viral particles released over time, we observed reduced virus production in our ETV7 KO cells
242 compared to control cells (**Fig. 4A**). This was the anticipated outcome because loss of a negative
243 regulator (i.e. ETV7) is expected to enhance expression of antiviral ISGs. We also measured
244 infectious viral titers and found a significant reduction in our ETV7 KO cells compared to control
245 cells (**Fig. S4A**). Using a fluorescent reporter strain of PR8 (PR8-mNeon) (*48*), we next visualized
246 infection and spread. As expected, we observed fewer cells expressing mNeon in ETV7 KO cells
247 using both microscopy (**Fig. 4B**) and flow cytometry readouts (**Fig. 4C**). We also tested whether
248 this phenotype would extend to a more contemporary H1N1 IAV strain, A/California/07/2009
249 (Cal/09), as well as an unrelated Victoria lineage influenza B virus strain, B/Malaysia/2506/2004
250 (Mal/04) (*49*). Using fluorescent reporter strains of these viruses, we observed significant
251 decreases in the number of Cal/09- and Mal/04-infected cells when comparing ETV7 KO cells to
252 control cells (**Fig. 4D and E**). In order to rule out non-IFN-related effects of ETV7 on inhibition
253 of influenza viral replication, we also performed these experiments with a non-influenza virus. We
254 selected Sendai virus (SeV) because, although it is known to induce a strong IFN response,

Figure 4

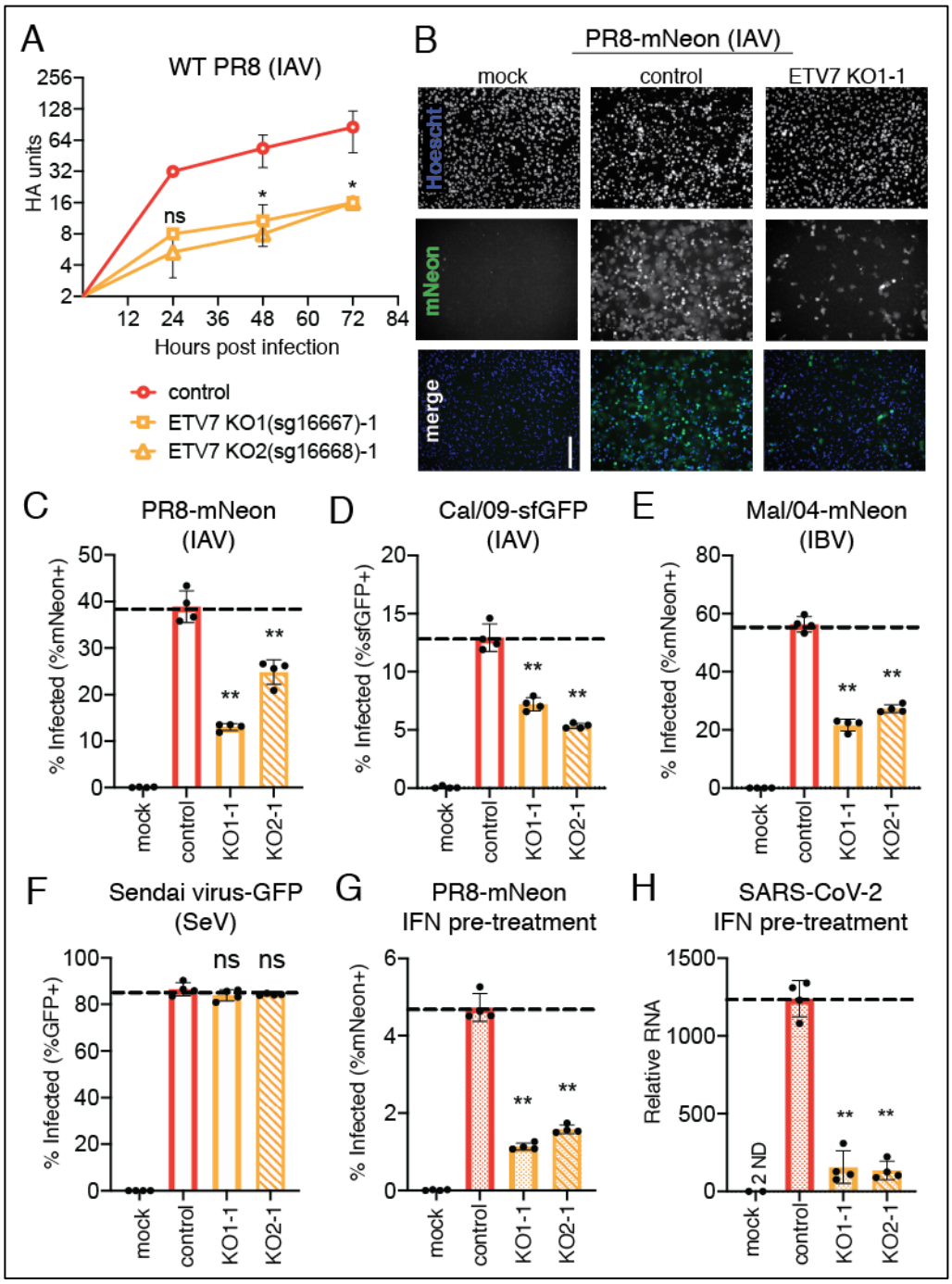

255

Fig. 4. Loss of ETV7 leads to restricted growth of multiple strains of influenza virus and SARS-CoV-2 with IFN treatment. (**A**) Hemagglutination (HA) assay of virus collected at indicated time points from non-targeting control and ETV7 KO A549 clonal cell lines after infection with WT PR8 virus (MOI=0.05, multicycle infection) (data shown as mean ± SD, n=3). (**B**) Control and ETV7 KO A549 clonal cell lines after mock or PR8-mNeon reporter virus infection (24 h, MOI=0.1, multicycle infection). Green = mNeon, blue = nuclei. Scale bar, 200 µm. (**C**) Flow cytometry quantification of control and ETV7 KO A549 clonal cell lines after infection with PR8-mNeon reporter virus (24 h, MOI=0.1, multicycle infection) (data shown as mean ± SD, n=4). (**D, E**) Percentage of infected (reporter+) cells from ETV7 KO A549 clonal cell lines compared to a control cell line after infection with (**D**) Cal/09-sfGFP or (**E**) Mal/04-mNeon

Fig. 4. (continued) reporter viruses (24 h, multicycle infection) (data shown as mean ± SD, n=4). (**F**) Percentage of infected (reporter+) cells from ETV7 KO A549 clonal cell lines compared to a control cell line after infection with Sendai-GFP reporter virus (24 h) (data shown as mean ± SD, n=4). (**G**) Percentage of infected (reporter+) cells from ETV7 KO A549 clonal cell lines compared to a control cell line after pre-treatment with IFN-α (100 U/ml, 6 h) then infection with PR8-mNeon reporter virus (24 h, MOI=0.1, multicycle) (data shown as mean ± SD, n=4). (**H**) qPCR detecting SARS-CoV-2 N vRNA in infected cells from ETV7 KO A549 clonal cell lines compared to a control cell line after pre-treatment with IFN-α (1000 U/ml, 6 h) then infection with SARS-CoV-2 virus (24 h, MOI=0.1) (data shown as mean ± SD, n=4). For all panels: P-values calculated using unpaired, two-tailed Student's t-tests (*p<0.05, **p<0.001) compared to infected, non-targeting sgRNA control samples.

256 previous reports (*50*) show SeV replication is relatively unaffected by type I IFN. Furthermore,
257 many of the ISGs most impacted by ETV7 have little to no effect against SeV, including IFITM1
258 (*51*), IFIT1 (*52*), and BST2/Tetherin (*53*). Using of a fluorescent reporter SeV, we observed no
259 significant change in the number of infected cells when comparing ETV7 KO cells to control cells
260 (**Fig. 4F**).
261
262 In addition to physiological induction of IFN after infection, exogenous IFN treatment is
263 frequently utilized or proposed as an antiviral therapy (*7*), either when there is difficulty
264 developing targeted antivirals (e.g. hepatitis C virus (*54*)) or there is an unexpected emergence of
265 a viral pathogen (e.g. swine or highly pathogenic avian influenza viruses (*55*), SARS-CoV (*56*),
266 Ebola virus (*57*), SARS-CoV-2 (*58–60*)). Therefore, we wanted to assess whether suppressing
267 ETV7 could be an effective strategy to enhance the antiviral effects of therapeutic IFN
268 administration. In support of this idea, we found treatment of ETV7 KO cells with IFN-α prior to
269 infection with PR8-mNeon led to an additional 5-fold enhancement of viral restriction compared
270 to IFN-treated WT control cells (**Fig. 4G**). Finally, since recent reports indicate that although
271 SARS-CoV-2 infections fail to induce a strong IFN responses (*61–63*), the virus is susceptible to
272 IFN treatment (*64–66*), we wanted to test if loss of ETV7 would potentiate IFN-mediated
273 suppression of SARS-CoV-2. With the same experimental design as the influenza virus

274 experiment, we found that pre-treatment of ETV7 KO cells with IFN-α resulted in a further 10-
275 fold reduction in SARS-CoV-2 vRNA compared to IFN-treated control cells (**Fig. 4H**). This
276 enhanced control was likely mediated via the ISG LY6E, which potently restricts SARS-CoV-2
277 (*67*, *68*) and we found to be regulated by ETV7 (**Fig. S4B**). Together, these experiments
278 demonstrate the potential of targeting ETV7 to enhance either the physiological or therapeutic
279 effects of IFN to control viral infection.
280

281 **Discussion**

282 In this study, we performed a CRISPR activation screen to identify negative regulators of the type
283 I IFN response. Specifically, we were interested in negative regulators that contribute to the types
284 of differentiated ISG profiles that are essential for effective control of viral infections. From this
285 screen, we identified ETV7 as a negative IFN regulator and subsequently showed it acts as a
286 transcription factor to repress subsets of ISGs through its recognized DNA binding motif. We also
287 demonstrated that the regulatory activity of ETV7 impacts the replication and spread of multiple
288 strains of influenza viruses. ETV7 loss also increased the antiviral effects of exogenous interferon
289 treatment against an H1N1 influenza virus and SARS-CoV-2. These findings demonstrate the
290 importance of ETV7 in fine-tuning the IFN response through specificity and transcriptional
291 repression to regulate antiviral ISG targets, and its potential as a target to enhance antiviral IFN-
292 based therapeutics.
293

294 ETV7 is a member of the ETS family of transcription factors. This family performs diverse
295 functions despite recognizing the same core DNA sequence, GGAA. Because these factors share
296 the same core motif, specificities are gained in other ways such as expression patterns (cell type,
297 basal expression, or immune pathway induction), active or repressive activity, and potential
298 binding partners (*69*, *70*). ETV7 is induced as an ISG and is repressive, whereas most ETS

299 transcription factors are activators, including ETS transcription factors recognized to assist in the
300 induction of ISG expression (e.g. ELF1 (*25*), PU.1 (*71*)). We also found repeatedly in our work
301 that the reporters and genes impacted by ETV7 contained ETS sites within ISRE sequences (**Fig.**
302 **2E-H, S2G-I, S4B**). This is not unexpected because it is recognized that many ETS family
303 members bind extended motifs similar to ISREs called ETS-IRF composite elements (EICE) (*72*).
304 EICE-associated activity is reported to require an IRF binding partner to direct ETS transcription
305 factor activity (*71*, *73*); therefore, it is likely ETV7 has an IRF binding partner. If ETV7 does
306 require a binding partner, this protein's induction and distribution likely contribute to the timing,
307 gene targets, and activity of ETV7 during the IFN response. It is known that IRFs can be basally
308 expressed (IRF2, IRF3), IFN-induced (IRF1, IRF7), or IFN-responsive (IRF9) (*72*), and the
309 availability of a binding partner could dramatically affect the timing and magnitude of effects on
310 EICE-controlled ISGs. Future work will define if ETV7 has specific binding partners and how
311 those interactions may contribute to the nonuniform, repressive activity of ETV7 during the type
312 I IFN response reported in this study.
313
314 IFN-induced regulators control the magnitude and duration of IFN responses in addition to the
315 temporal regulation of specific waves of ISGs (*74*). These coordinated waves of ISG induction can
316 peak early or late during the IFN response and are thought to correspond to specific stages of virus
317 replication or immune processes (*1*, *6*). We compared the induction of ETV7 with IFI44L, IFIT1,
318 ISG15 and RSAD2, and we observed ETV7 is upregulated at earlier time points than these
319 prototypical ISGs (**Fig. 3A**). We expanded our analysis to published datasets of human gene
320 expression during respiratory infections and concluded that ETV7 is generally induced earlier than
321 many ISGs (*75*). Although not the focus of our study, ETV7's early induction pattern suggests it
322 may be a key regulator of the first stages of IFN-mediated gene induction. We favor a model

323 wherein early ETV7 expression is responsible for reducing the accumulation, or delaying the
324 expression, of ISGs controlled by ISREs and promoters containing ETS motifs.
325
326 ETV7 is induced during infections across many vertebrate species (*76*, *77*), indicating a potential
327 conserved, relevant role in the immune response; however, ETV7 has been lost in mice and closely
328 related rodents (*78*). Since mice and rodents have an intact interferon response pathway, a natural
329 question is: how are the activities of ETV7 being accounted for in these animals? While we have
330 no clear answer from the data in this study, it is well-recognized that IFN responses contain many
331 redundancies (*41*). Accordingly, we believe other ETS family members, potentially the closely
332 related ETV6 (which is also induced by IFNs), may perform the role of ETV7 in mice (*79*). Future
333 studies will be required to test the hypothesis that mice induce an ETV7-related alternative during
334 the type I IFN response.
335
336 Another important question is why the IFN-induced activity of ETV7 has been maintained
337 throughout evolution. In this report, we provide evidence that ETV7's activity reduces a cell's
338 ability to restrict virus infection; this seems counterintuitive to ETV7 benefitting the host. We
339 hypothesize that regulators like ETV7 are important to prevent excessive inflammatory signaling.
340 It is appreciated that negative regulators of the IFN response are required to prevent extreme and
341 prolonged immune responses, which are associated with poor disease outcomes after infection
342 (*80–82*). ETV7 potentially contributes to the cumulative activities of negative IFN regulators to
343 limit IFN responses during pathogen clearance. Additionally, it stands to reason that individual
344 ISGs have different toxic effects on the cell. It is tempting to speculate that ETV7 suppresses ISGs
345 whose accumulation is particularly harmful to cell viability and host recovery after infection.
346

347 Additionally, the relevance of controlled IFN responses goes beyond infectious disease; patients
348 with dysfunctional USP18, a negative regulator of the IFN response, develop a type I
349 interferonopathy that results in a severe pseudo-TORCH (Toxoplasmosis, Other agents, Rubella,
350 Cytomegalovirus, and Herpes simplex) syndrome (*83*). Mouse knockouts for other negative
351 regulators of the IFN response (SOCS1, SOCS3, USP18) also develop non-pathogen associated,
352 chronic inflammatory diseases (*84–87*). ETV7's lack of a murine homolog eliminates an easily
353 generated animal knockout model to experimentally show ETV7's relevance as a general innate
354 immune repressor. However, genome-wide association studies (GWAS) have linked ETV7 to
355 autoimmune diseases including rheumatoid arthritis and multiple sclerosis (*88*, *89*); both of these
356 autoimmune diseases have evidence of enhanced ISG expression (*90*, *91*). Thus, although the
357 specific contributions of ETV7 activity to IFN regulation are currently undefined, its potential role
358 is not limited to viral infections.
359
360 In conclusion, this study identified ETV7 as a negative regulator of the type I IFN response.
361 Previously, ETV7 was appreciated to be an ISG; however, a specific function during the IFN
362 response was unknown. We determined that ETV7 acts as a transcription factor to target specific
363 ISGs for repression, potentially contributing to the complex ISG transcriptional landscape.
364 Additionally, many of the ETV7-regulated ISGs restrict respiratory viruses (*42*, *67*, *68*), and we
365 showed that loss of ETV7 can further enhance the ability of type I IFN to control influenza virus
366 and SARS-CoV-2 replication. Further work is required to understand the complexity of IFN
367 regulation, while therapeutic targeting of factors like ETV7 could lead to the development of a
368 new class of host-directed antivirals that can enhance or tailor ISG responses to specific viruses.

369 **Materials and Methods**

370 *Cloning*

371 To generate reporters sensitive to IFN, we designed gBlocks (IDT) containing ISREs to be cloned
372 into the pTRIP vector ahead of a minimal CMV promoter controlling expression of sfGFP. To
373 clone and express the open reading frames (ORFs) of our screen hits, we designed primers for
374 cloning into the pLEX-MCS vector using Gibson Assembly (NEB). To amplify ETV7, NUP153
375 and USP18 we used cDNA templates from Transomic Technologies. To amplify C1GALT1 and
376 EIF2AK1 we used RNA from IFN-stimulated A549 cells. The DNA binding mutant ETV7,
377 ETV7(KALK) (*35*), and codon-optimized SOCS1 expression plasmids were generated using a
378 gBlock (IDT). FLAG-tagged ETV7, ETV7(FLAG), was generated using a primer including the
379 FLAG tag. Non-targeting and ETV7-targeting CRISPR KO sgRNAs were cloned by annealing
380 oligos encoding the desired sgRNA sequence and ligating them directly into the lentiCRISPRv2
381 vector (Addgene). DNA was transformed into NEB 5-alpha high efficiency competent cells. Insert
382 size was verified with PCR and purified plasmids were sequenced using Sanger sequencing.

383

384 *Cells*

385 All cells were obtained from ATCC and grown at 37°C in 5% CO_2. A549 and 293T cells were
386 grown in Dulbecco's Modified Eagle Medium (DMEM) supplemented with 5% fetal bovine
387 serum, GlutaMAX, and penicillin-streptomycin. Madin-Darby canine kidney (MDCK) cells were
388 grown in minimal essential media (MEM) supplemented with 5% fetal bovine serum, HEPES,
389 $NaHCO_3$, GlutaMAX, and penicillin-streptomycin. The A549 CRISPR-SAM cells were
390 previously validated (*92*) and transduced with the IFN response reporter three times before being
391 clonally selected. The A549 CRISPR KO cells were transduced (ETV7 KO1 = sg16667, ETV7
392 KO2 = sg16668, nontargeting control) and then selected using puromycin (10 μg/mL). A549-IFN
393 response reporter ETV7 KO lines were selected with puromycin and used as pooled lines. A549

ETV7 KO lines were selected with puromycin and subsequently plated at a dilution to isolate single cells, which were grown until colonies of an appropriate size allowed for collection. These clonally selected colonies were grown up and verified to be KO lines (control, KO1-1, KO1-2, KO2-1, KO2-2) by sequencing the DNA lesions generated as a result of Cas9 endonuclease activity, results shown below. Guide sequences = underlined, insertions = bolded, deletions = dashes, exonic sequences = uppercase, intronic sequences = lowercase.

ETV7 KO guide 1 (sg16667)

WT	5' CTG CCA TGC ACC G<u>CG GAG CAC GGG TTC GAG ATG</u> AAC GGA CGC GCC 3'
	protein length = 342aa
KO1-1 allele 1	5' CTG CCA TGC ACC GCG GA**A** GCA CGG GTT CGA GAT GAA CGG ACG CGC 3'
	predicted protein length = 104aa
KO1-1 allele 2	5' CTG CCA TGC ACC GCG GA**A** GCA CGG GTT CGA GAT GAA CGG ACG CGC 3'
	predicted protein length = 104aa
KO1-2 allele 1	5' CTG CCA TGC ACC GCG GA**A** GCA CGG GTT CGA GAT GAA CGG ACG CGC 3'
	predicted protein length = 104aa
KO1-2 allele 2	5' CTG CCA TGC ACC GCG GA**A** GCA CGG GTT CGA GAT GAA CGG ACG CGC 3'
	predicted protein length = 104aa

ETV7 KO guide 2 (sg16668)

WT	5' GCG ATG CCG CAG GCC <u>CCC ATT GAC GGC AGG ATC GC</u>T Ggtgagtgggagg 3'
	protein length = 342aa
KO2-1 allele 1	5' GCG ATG CCG CAG GCC CCC ATT GAC G-- --- --- -CT Ggtgagtgggagg 3'
	predicted protein length = 333aa
KO2-1 allele 2	5' GCG ATG CCG CAG GCC CCC ATT GAC GGC AGG --- --- --tgagtgggagg 3'
	predicted protein length = unknown, loss of splice site
KO2-2 allele 1	5' GCG ATG CCG CAG GCC CCC ATT GAC G-- --- --- -CT Ggtgagtgggagg 3'
	predicted protein length = 333aa
KO2-2 allele 2	5' GCG ATG CCG CAG GCC CCC ATT GAC GGC AGG -T**GA** CGC TGgtgagtgggagg 3'
	predicted protein length = 220aa

Flow Cytometry

Cells were trypsinized and analyzed on a Fortessa X-20 (BD) machine with standard laser and filter combinations. Data was visualized and processed with FlowJo software.

CRISPR Activation Screen

434 The sgRNA library was packaged into lentivirus as previously described (*92*). After packaging
435 and titering the lentivirus, $2x10^8$ A549-CRISPR-SAM-IFN response reporter cells were seeded
436 onto 15 cm plates (10 plates total). The next day they were transduced with the packaged sgRNA
437 library (MOI=0.5). After 48 h, the transduced cells were split and half were collected as a
438 transduction control, while the remaining half were plated back onto 15 cm plates. The next day,
439 cells were treated with IFN-α ($4x10^3$ U/mL) for 6 h. Cells were then collected and sorted on a
440 Beckman Coulter Astrios cell sorter. Specifically, gates were set to sort GFP-negative cells as the
441 population of interest, as well as GFP-positive cells as a control population of cells still capable of
442 signaling. This screen was performed in duplicate. Genomic DNA was extracted from sorted cells
443 using the Zymo Quick gDNA micro prep kit. PCR was subsequently performed using barcoded
444 primers as previously described using the NEB Next High Fidelity 2x PCR master mix (*92*). PCR
445 bands were gel purified using the Thermo GeneJET gel extraction kit. Samples were then
446 sequenced via next-generation Illumina MiSeq using paired-end 150 bp reads.
447
448 *Screen Analysis*
449 Raw MiSeq read files were aligned to the CRISPR SAM sgRNA library and raw reads for each
450 sgRNA were counted using the MAGeCK pipeline (*29*). sgRNA enrichment was determined using
451 the generated count files and the MAGeCK-MLE analysis pipeline. Genes were sorted based on
452 z-score and determined to be significantly enriched if their z-score was at least two standard
453 deviations above the average z-score of the entire sorted population.
454
455 *Western Blotting*
456 Cells were trypsinized and $1x10^6$ cells were pelleted at 800 x g for 5 min. Equal amounts of cellular
457 material were loaded into 4-20% acrylamide gels (Bio-Rad) and imaged using a ChemiDoc
458 Imaging System (Bio-Rad). Protein was transferred to a nitrocellulose membrane at 60V for 60

459 min. PBS with 5% (w/v) non-fat dried milk and 0.1% Tween-20 were used to block for 1 h at 4°C.
460 Primary antibodies were then incubated with the membrane overnight at 4°C. Antibodies used
461 were rabbit anti-ETV7 (Sigma, HPA029033), rabbit anti-IFIT1 (Cell Signaling, D2X9Z), mouse
462 anti-FLAG (Sigma, F3165) and mouse anti-αtubulin (Sigma, T5168). Membranes were washed
463 five times in PBS with 0.1% Tween-20 and then an anti-rabbit-HRP (Thermo, A16104) or anti-
464 mouse-HRP (Thermo, A16072) secondary antibody was added for 1 h. The membrane was then
465 washed five times and Clarity or Clarity Max ECL substrate (Bio-Rad) was added before being
466 exposed to film and developed.
467
468 *RT-qPCR*
469 For all experiments except SARS-CoV-2 infection experiments, total RNA was collected and
470 prepared using Monarch Total RNA Miniprep Kits (NEB). For SARS-CoV-2 experiments, cells
471 were collected in TRIzol (Invitrogen) and RNA was isolated using Phasemaker tubes (Invitrogen).
472 One-step RT-qPCR was performed with commercial TaqMan assays from Thermo for ETV7
473 (Hs00903229_m1), C1GALT1 (Hs00863329_g1), NUP153 (Hs01018919_m1), ISG15
474 (Hs00196051_m1), MX1 (Hs00895608_m1), IFIT1 (Hs00356631_g1), IFI44L
475 (Hs00915292_m1), RSAD2 (Hs00895608_m1), IFITM1 (Hs00705137_s1), OAS1
476 (Hs00973635_m1), IFIT2 (Hs00533665_m1), IFIT3 (Hs01922752_s1), IFI44 (Hs00197427_m1),
477 BST2 (Hs01561315_m1), and ACTB (Hs01060665_g1) and primers/probe from BEI targeting the
478 SARS-CoV-2 N region using the EXPRESS One-Step Superscript qRT-PCR Kit on an Applied
479 Biosystems StepOnePlus or QuantStudio 3 instrument. RNA was normalized using an endogenous
480 18S rRNA primer/probe set (Applied Biosystems).
481
482 *DNA pull-down assay*

483 Nuclear extract from 293T cells expressing ETV7 and treated with IFN-α (100 U/mL, 9 h) was
484 generated using NE-PER extraction reagents (Thermo Scientific). This nuclear extract was
485 incubated with poly(dI-dC) as nonspecific competitor DNA, 10x ligase buffer (Invitrogen), 200
486 mM EDTA, biotinylated DNA bait (either WT or -ETS ISG15 ISRE (*93*)), and 20x excess
487 nonbiotinylated DNA competitor for 30 min at room temperature. This mixture was then incubated
488 with streptavidin-coated magnetic beads (Invitrogen), followed by four washes with TTBS.
489 Proteins bound to the biotinylated DNA bait captured by the streptavidin beads were eluted with
490 protein sample buffer and then detected by Western blot. Input (nuclear extract) was diluted 1:200
491 for loading. No bait (control) contained no biotinylated DNA.
492
493 *RNA sequencing*
494 293T cells were transfected with ETV7- or control-expressing plasmids and selected using
495 puromycin (20 μg/mL) for 24 h before treatment with IFN-α (100 U/mL). Total RNA was
496 collected at 9 h post-IFN treatment using Monarch Total RNA Miniprep Kits (NEB). RNA was
497 prepped for RNA sequencing submission using the NEBNext Poly(A) mRNA Magnetic Isolation
498 Module (NEB), NEBNext Ultra II RNA Library Prep Kit for Illumina (NEB), and NEBNext
499 Multiplex Oligos for Illumina (NEB). Samples were analyzed on one lane of an Illumina HiSeq
500 4000 using 50 bp single strand reads. Mapping of the raw reads to the human hg19 reference
501 genome was accomplished using a custom application on the Illumina BaseSpace Sequence Hub
502 (*94*). After data normalization, average read values were compared across samples. For
503 comparisons in which some samples had zero reads detected for a specific gene, one read was
504 added to all values in the sample to complete analyses that required non-zero values. The heat map
505 shows genes upregulated 2.5-fold (after normalization) with IFN treatment in the control samples.
506 Values shown are z-scores.
507

508 *ChIP-qPCR*

509 293T cells were transfected with a FLAG-tagged ETV7-expressing plasmid, ETV7(FLAG), 48 h
510 before treatment with IFN-α (100 U/mL, 9 h). Chromatin immunoprecipitation was performed
511 using the ChIP-IT Express Enzymatic kit according to the manufacturer's directions (Active
512 Motif). DNA was enzymatically sheared for 10 min. ChIP antibodies included mouse IgG (Active
513 Motif), rabbit anti-FLAG (Cell Signaling, 14793S), and mouse anti-FLAG (Sigma, F3165).
514 Quantitative PCR was performed using SYBR Green (Bio-Rad) and primers targeting the Chr12
515 gene desert (Active Motif) or IFI44L promoter (forward primer = 5'
516 TTTCATGCCTGCCTACATAC 3', reverse primer = 5' ATGCCAACTGCCACTAAC 3') in a
517 region containing two potential ISRE sequences overlapping with ETS sites, and analyzed using
518 the ChIP-IT qPCR Analysis kit (Active Motif).

519

520 *Viruses*

521 PR8-mNeon was generated via insertion of the mNeon fluorescent gene (*95*) into segment 4 of the
522 virus (*48*). Mal/04-mNeon was generated by inserting the mNeon fluorescent gene (*95*) into
523 segment 4 of the Mal/04 genome (*49*). Cal/09-sfGFP was generated via insertion of the sfGFP
524 gene (*96*) into segment 8 of the virus using the same scheme previously used to insert Cre
525 recombinase (*97*). Sendai-GFP was a gift from Benhur Lee (*98*). For influenza virus infections,
526 cells were either mock- or virus-infected for 1 h and then cultured in OptiMEM supplemented with
527 bovine serum albumin (BSA), penicillin-streptomycin, and 0.2 μg/mL TPCK-treated trypsin
528 protease (Sigma). For Sendai infections, cells were infected for 1 h and then cultured in DMEM.
529 For SARS-CoV-2 infections, cells were washed with PBS before infection with SARS-CoV-
530 2 isolate USA-WA1/2020 from BEI Resources in 2% FBS DMEM infection media for 1 hour.
531 PR8 WT, PR8-mNeon, Cal/09-sfGFP, Sendai-GFP, and SARS-CoV-2 were incubated at 37°C,
532 Mal/04-mNeon was incubated at 33°C.

533

534 *Viral Growth Assays*

535 Hemagglutination (HA) assays to measure the number of viral particles were performed by diluting
536 influenza infected cell supernatants collected at the indicated time points in cold PBS. An equal
537 amount of chicken blood diluted 1:40 in PBS was mixed with serially diluted virus and incubated
538 at 4°C for 2-3 h before scoring. Infectious viral titers were determined using standard plaque assay
539 procedures on MDCK cells. Infected cell supernatants were collected at 18 h, serially diluted, and
540 used to infect confluent 6-well plates for 1 h before removing the virus and adding the agar overlay.
541 Cells were then incubated at 37°C for 48 h before being fixed in 4% PFA overnight. The 4% PFA
542 was then aspirated, and the agar layer was removed before washing cells with PBS. Serum from
543 WT PR8 infected mice was diluted 1:2,000 in antibody dilution buffer (5% (w/v) non-fat dried
544 milk and 0.05% Tween-20 in PBS) and incubated on cells at 4°C overnight. Cells were then
545 washed twice with PBS and incubated for 1 h with anti-mouse IgG horseradish peroxidase (HRP)-
546 conjugated sheep antibody (GE Healthcare) diluted 1:4,000 in antibody dilution buffer. Assays
547 were then washed twice with PBS and exposed to 0.5 mL of TrueBlue peroxidase substrate (KPL)
548 for 20 min. Plates were then washed with water and dried before plaques were counted.

549
550

551 **Supplementary Materials**
552
553 Fig. S1. CRISPR activation screen hit identification and validation.
554
555 Fig. S2. ETV7 represses IFN-stimulated expression and directly binds an ISG promoter.
556
557 Fig. S3. ETV7 loss increases IFN-stimulated expression.
558
559 Fig. S4. ETV7 loss results in decreased viral titers and increased antiviral gene expression.
560
561 Table S1. Hits from CRISPRa screen for negative regulators of the type I IFN response.
562
563 Table S2. ISRE sequences identified in the literature.
564
565 Table S3. Gene set enrichment analysis of 200 most downregulated genes in ETV7-
566 expressing cells without IFN treatment.
567
568 Table S4. Gene set enrichment analysis of 200 most downregulated genes in ETV7-
569 expressing cells after 9hr IFN treatment.
570
571 Data file S1. CRISPRa screen for negative regulators of the type I IFN response
572 sgRNA sequences, transduction read counts, and screen read counts.
573
574 Data file S2. CRISPRa screen for negative regulators of the type I IFN response
575 MAGeCK z-scores and potential hit cutoffs.
576
577 Data file S3. RNA sequencing with ETV7 overexpression and IFN treatment
578 reads and results.
579

References

580 1. W. M. Schneider, M. D. Chevillotte, C. M. Rice, Interferon-Stimulated Genes: A
581 Complex Web of Host Defenses. *Annu. Rev. Immunol.* **32**, 513–545 (2014).
582 2. J. W. Schoggins, Interferon-Stimulated Genes: What Do They All Do? *Annu. Rev. Virol.*
583 **6**, 567–584 (2019).
584 3. J. W. Schoggins, S. J. Wilson, M. Panis, M. Y. Murphy, C. T. Jones, P. Bieniasz, C. M.
585 Rice, A diverse range of gene products are effectors of the type I interferon antiviral
586 response. *Nature*. **472**, 481–485 (2011).
587 4. J. W. Schoggins, D. A. MacDuff, N. Imanaka, M. D. Gainey, B. Shrestha, J. L. Eitson, K.
588 B. Mar, R. B. Richardson, A. V. Ratushny, V. Litvak, R. Dabelic, B. Manicassamy, J. D.
589 Aitchison, A. Aderem, R. M. Elliott, A. García-Sastre, V. Racaniello, E. J. Snijder, W. M.
590 Yokoyama, M. S. Diamond, H. W. Virgin, C. M. Rice, Pan-viral specificity of IFN-
591 induced genes reveals new roles for cGAS in innate immunity. *Nature*. **505**, 691–695
592 (2014).
593 5. M. Kane, T. M. Zang, S. J. Rihn, C. M. Rice, S. J. Wilson, P. D. Bieniasz, Identification
594 of Interferon-Stimulated Genes with Antiretroviral Activity. *Cell Host Microbe*. **20**, 392–
595 405 (2016).
596 6. E. V. Mesev, R. A. LeDesma, A. Ploss, Decoding type I and III interferon signalling
597 during viral infection. *Nat. Microbiol.* **4**, 914–924 (2019).
598 7. B. X. Wang, E. N. Fish, The yin and yang of viruses and interferons. *Trends Immunol.* **33**
599 (2012), doi:10.1016/j.it.2012.01.004.
600 8. G. R. Stark, J. E. Darnell, The JAK-STAT Pathway at Twenty. *Immunity*. **36**, 503–514
601 (2012).
602 9. K. Honda, H. Yanai, A. Takaoka, T. Taniguchi, Regulation of the type I IFN induction: a
603 current view. *Int. Immunol.* **17**, 1367–1378 (2005).
604 10. D. E. Levy, D. S. Kessler, R. Pine, N. Reich, J. E. Darnell, Interferon-induced nuclear
605 factors that bind a shared promoter element correlate with positive and negative
606 transcriptional control. *Genes Dev.* **2**, 383–93 (1988).
607 11. N. P. D. Liau, A. Laktyushin, I. S. Lucet, J. M. Murphy, S. Yao, E. Whitlock, K.
608 Callaghan, N. A. Nicola, N. J. Kershaw, J. J. Babon, The molecular basis of JAK/STAT
609 inhibition by SOCS1. *Nat. Commun.* **9**, 1558 (2018).
610 12. M. P. Malakhov, O. A. Malakhova, K. Il Kim, K. J. Ritchie, D.-E. Zhang, UBP43
611 (USP18) specifically removes ISG15 from conjugated proteins. *J. Biol. Chem.* **277**, 9976–
612 81 (2002).
613 13. K.-I. Arimoto, S. Miyauchi, S. A. Stoner, J.-B. Fan, D.-E. Zhang, Negative regulation of
614 type I IFN signaling. *J. Leukoc. Biol.* **103**, 1099–1116 (2018).
615 14. G. Randall, L. Chen, M. Panis, A. K. Fischer, B. D. Lindenbach, J. Sun, J. Heathcote, C.
616 M. Rice, A. M. Edwards, I. D. McGilvray, Silencing of USP18 Potentiates the Antiviral
617 Activity of Interferon Against Hepatitis C Virus Infection. *Gastroenterology*. **131**, 1584–
618 1591 (2006).
619 15. K. G. Frey, C. M. I. Ahmed, R. Dabelic, L. D. Jager, E. N. Noon-Song, S. M. Haider, H.
620 M. Johnson, N. J. Bigley, HSV-1-induced SOCS-1 expression in keratinocytes: use of a
621 SOCS-1 antagonist to block a novel mechanism of viral immune evasion. *J. Immunol.*
622 **183**, 1253–62 (2009).
623 16. C. J. Carbone, H. Zheng, S. Bhattacharya, J. R. Lewis, A. M. Reiter, P. Henthorn, Z.-Y.
624 Zhang, D. P. Baker, R. Ukkiramapandian, K. K. Bence, S. Y. Fuchs, Protein tyrosine
625 phosphatase 1B is a key regulator of IFNAR1 endocytosis and a target for antiviral
626 therapies. *Proc. Natl. Acad. Sci. U. S. A.* **109**, 19226–31 (2012).

627 17. M. Sa Ribero, N. Jouvenet, M. Dreux, S. Nisole, Interplay between SARS-CoV-2 and the
628 type I interferon response. *PLOS Pathog.* **16**, e1008737 (2020).
629 18. J. R. Teijaro, S. Studer, N. Leaf, W. B. Kiosses, N. Nguyen, K. Matsuki, H. Negishi, T.
630 Taniguchi, M. B. A. Oldstone, H. Rosen, S1PR1-mediated IFNAR1 degradation
631 modulates plasmacytoid dendritic cell interferon-α autoamplification. *Proc. Natl. Acad.*
632 *Sci. U. S. A.* **113**, 1351–6 (2016).
633 19. K. B. Walsh, J. R. Teijaro, P. R. Wilker, A. Jatzek, D. M. Fremgen, S. C. Das, T.
634 Watanabe, M. Hatta, K. Shinya, M. Suresh, Y. Kawaoka, H. Rosen, M. B. A. Oldstone,
635 Suppression of cytokine storm with a sphingosine analog provides protection against
636 pathogenic influenza virus. *Proc. Natl. Acad. Sci. U. S. A.* **108**, 12018–23 (2011).
637 20. F. Naz, M. Arish, Battling COVID-19 Pandemic: Sphingosine-1-Phosphate Analogs as an
638 Adjunctive Therapy? *Front. Immunol.* **11**, 1102 (2020).
639 21. P. J. Hertzog, B. R. G. Williams, Fine tuning type I interferon responses. *Cytokine Growth*
640 *Factor Rev.* **24**, 217–225 (2013).
641 22. J. P. B. Viola, R. P. Donnelly, H. M. Johnson, H. A. R. Bluyssen, A. Michalska, K.
642 Blaszczyk, J. Wesoly, A Positive Feedback Amplifier Circuit That Regulates Interferon
643 (IFN)-Stimulated Gene Expression and Controls Type I and Type II IFN Responses. **9**, 28
644 (2018).
645 23. N. Tanaka, T. Kawakami, T. Taniguchi, Recognition DNA sequences of interferon
646 regulatory factor 1 (IRF-1) and IRF-2, regulators of cell growth and the interferon system.
647 *Mol. Cell. Biol.* **13**, 4531–8 (1993).
648 24. M. Sato, N. Hata, M. Asagiri, T. Nakaya, T. Taniguchi, N. Tanaka, Positive feedback
649 regulation of type I *IFN* genes by the IFN-inducible transcription factor IRF-7. *FEBS Lett.*
650 **441**, 106–110 (1998).
651 25. L. L. Seifert, C. Si, D. Saha, M. Sadic, M. de Vries, S. Ballentine, A. Briley, G. Wang, A.
652 M. Valero-Jimenez, A. Mohamed, U. Schaefer, H. M. Moulton, A. García-Sastre, S.
653 Tripathi, B. R. Rosenberg, M. Dittmann, The ETS transcription factor ELF1 regulates a
654 broadly antiviral program distinct from the type I interferon response. *PLOS Pathog.* **15**,
655 e1007634 (2019).
656 26. P. Hubel, C. Urban, V. Bergant, W. M. Schneider, B. Knauer, A. Stukalov, P. Scaturro, A.
657 Mann, L. Brunotte, H. H. Hoffmann, J. W. Schoggins, M. Schwemmle, M. Mann, C. M.
658 Rice, A. Pichlmair, A protein-interaction network of interferon-stimulated genes extends
659 the innate immune system landscape. *Nat. Immunol.* **20**, 493–502 (2019).
660 27. X. Li, X. Zhao, Y. Fang, X. Jiang, T. Duong, C. Fan, C.-C. Huang, S. R. Kain, Generation
661 of Destabilized Green Fluorescent Protein as a Transcription Reporter. *J. Biol. Chem.* **273**,
662 34970–34975 (1998).
663 28. S. Konermann, M. D. Brigham, A. E. Trevino, J. Joung, O. O. Abudayyeh, C. Barcena, P.
664 D. Hsu, N. Habib, J. S. Gootenberg, H. Nishimasu, O. Nureki, F. Zhang, Genome-scale
665 transcriptional activation by an engineered CRISPR-Cas9 complex. *Nature*. **517**, 583–8
666 (2015).
667 29. W. Li, H. Xu, T. Xiao, L. Cong, M. I. Love, F. Zhang, R. A. Irizarry, J. S. Liu, M. Brown,
668 X. S. Liu, MAGeCK enables robust identification of essential genes from genome-scale
669 CRISPR/Cas9 knockout screens. *Genome Biol.* **15**, 554 (2014).
670 30. I. Rusinova, S. Forster, S. Yu, A. Kannan, M. Masse, H. Cumming, R. Chapman, P. J.
671 Hertzog, INTERFEROME v2.0: an updated database of annotated interferon-regulated
672 genes. *Nucleic Acids Res.* **41**, D1040–D1046 (2012).
673 31. A.-P. Han, C. Yu, L. Lu, Y. Fujiwara, C. Browne, G. Chin, M. Fleming, P. Leboulch, S.
674 H. Orkin, J. Chen, Heme-regulated eIF2alpha kinase (HRI) is required for translational
675 regulation and survival of erythroid precursors in iron deficiency. *EMBO J.* **20**, 6909–

676 6918 (2001).
677 32. A. Marg, Y. Shan, T. Meyer, T. Meissner, M. Brandenburg, U. Vinkemeier,
678 Nucleocytoplasmic shuttling by nucleoporins Nup153 and Nup214 and CRM1-dependent
679 nuclear export control the subcellular distribution of latent Stat1. *J. Cell Biol.* **165**, 823–33
680 (2004).
681 33. M. D. Potter, A. Buijs, B. Kreider, L. van Rompaey, G. C. Grosveld, Identification and
682 characterization of a new human ETS-family transcription factor, TEL2, that is expressed
683 in hematopoietic tissues and can associate with TEL1/ETV6. *Blood*. **95**, 3341–8 (2000).
684 34. H. Poirel, R. G. Lopez, V. Lacronique, V. Della Valle, M. Mauchauffé, R. Berger, J.
685 Ghysdael, O. A. Bernard, Characterization of a novel ETS gene, TELB, encoding a
686 protein structurally and functionaly related to TEL. *Oncogene*. **19**, 4802–4806 (2000).
687 35. F. C. Harwood, R. I. Klein Geltink, B. P. O'Hara, M. Cardone, L. Janke, D. Finkelstein, I.
688 Entin, L. Paul, P. J. Houghton, G. C. Grosveld, ETV7 is an essential component of a
689 rapamycin-insensitive mTOR complex in cancer. *Sci. Adv.* **4**, eaar3938 (2018).
690 36. H. Wei, G. Badis, M. F. Berger, T. Kivioja, K. Palin, M. Enge, M. Bonke, A. Jolma, M.
691 Varjosalo, A. R. Gehrke, J. Yan, S. Talukder, M. Turunen, M. Taipale, H. G.
692 Stunnenberg, E. Ukkonen, T. R. Hughes, M. L. Bulyk, J. Taipale, Genome-wide analysis
693 of ETS-family DNA-binding in vitro and in vivo. *EMBO J.* **29**, 2147–2160 (2010).
694 37. J. Reimand, T. Arak, P. Adler, L. Kolberg, S. Reisberg, H. Peterson, J. Vilo, g:Profiler-a
695 web server for functional interpretation of gene lists (2016 update). *Nucleic Acids Res.* **44**,
696 W83–W89 (2016).
697 38. N. E. Sanjana, O. Shalem, F. Zhang, Improved vectors and genome-wide libraries for
698 CRISPR screening. *Nat. Methods*. **11**, 783–784 (2014).
699 39. D. C. Busse, D. Habgood-Coote, S. Clare, C. Brandt, I. Bassano, M. Kaforou, M. Levin,
700 J.-F. Eleouet, P. Kellam, J. S. Tregoning, Interferon-induced Protein-44 and Interferon-
701 induced Protein 44-like restrict 1 replication of Respiratory Syncytial Virus 2 Downloaded
702 from. *J. Virol* (2020), doi:10.1128/JVI.00297-20.
703 40. D. J. Morales, D. J. Lenschow, The antiviral activities of ISG15. *J. Mol. Biol.* **425**, 4995–
704 5008 (2013).
705 41. J. W. Schoggins, Recent advances in antiviral interferon-stimulated gene biology.
706 *F1000Research*. **7**, 309 (2018).
707 42. A. García-Sastre, Induction and evasion of type I interferon responses by influenza
708 viruses. *Virus Res.* **162**, 12–18 (2011).
709 43. A. L. Brass, I.-C. Huang, Y. Benita, S. P. John, M. N. Krishnan, E. M. Feeley, B. J. Ryan,
710 J. L. Weyer, L. van der Weyden, E. Fikrig, D. J. Adams, R. J. Xavier, M. Farzan, S. J.
711 Elledge, The IFITM Proteins Mediate Cellular Resistance to Influenza A H1N1 Virus,
712 West Nile Virus, and Dengue Virus. *Cell*. **139**, 1243–1254 (2009).
713 44. Y. Li, S. Banerjee, Y. Wang, S. A. Goldstein, B. Dong, C. Gaughan, R. H. Silverman, S.
714 R. Weiss, Activation of RNase L is dependent on OAS3 expression during infection with
715 diverse human viruses. *Proc. Natl. Acad. Sci. U. S. A.* **113**, 2241–6 (2016).
716 45. A. Pichlmair, C. Lassnig, C.-A. Eberle, M. W. Górna, C. L. Baumann, T. R. Burkard, T.
717 Bürckstümmer, A. Stefanovic, S. Krieger, K. L. Bennett, T. Rülicke, F. Weber, J. Colinge,
718 M. Müller, G. Superti-Furga, IFIT1 is an antiviral protein that recognizes 5′-triphosphate
719 RNA. *Nat. Immunol.* **12**, 624–630 (2011).
720 46. M. A. Yondola, F. Fernandes, A. Belicha-Villanueva, M. Uccelini, Q. Gao, C. Carter, P.
721 Palese, Budding capability of the influenza virus neuraminidase can be modulated by
722 tetherin. *J. Virol.* **85**, 2480–91 (2011).
723 47. X. Wang, E. R. Hinson, P. Cresswell, The Interferon-Inducible Protein Viperin Inhibits
724 Influenza Virus Release by Perturbing Lipid Rafts. *Cell Host Microbe*. **2**, 96–105 (2007).

725 48. A. T. Harding, B. E. Heaton, R. E. Dumm, N. S. Heaton, Rationally Designed Influenza
726 Virus Vaccines That Are Antigenically Stable during Growth in Eggs. *MBio*. **8** (2017),
727 doi:10.1128/mBio.00669-17.
728 49. R. E. Dumm, J. K. Fiege, B. M. Waring, C. T. Kuo, R. A. Langlois, N. S. Heaton, Non-
729 lytic clearance of influenza B virus from infected cells preserves epithelial barrier
730 function. *Nat. Commun.* **10**, 779 (2019).
731 50. J. R. Bedsaul, L. A. Zaritsky, K. C. Zoon, Type I interferon-mediated induction of
732 antiviral genes and proteins fails to protect cells from the cytopathic effects of sendai virus
733 infection. *J. Interf. Cytokine Res.* **36**, 652–665 (2016).
734 51. J. M. Perreira, C. R. Chin, E. M. Feeley, A. L. Brass, IFITMs restrict the replication of
735 multiple pathogenic viruses. *J. Mol. Biol.* **425** (2013), pp. 4937–4955.
736 52. D. F. Young, J. Andrejeva, X. Li, F. Inesta-Vaquera, C. Dong, V. H. Cowling, S.
737 Goodbourn, R. E. Randall, Human IFIT1 Inhibits mRNA Translation of Rubulaviruses but
738 Not Other Members of the Paramyxoviridae Family. *J. Virol.* **90**, 9446–9456 (2016).
739 53. C. Bampi, L. Rasga, L. Roux, Antagonism to human BST-2/tetherin by Sendai virus
740 glycoproteins. *J. Gen. Virol.* **94**, 1211–9 (2013).
741 54. M. P. Manns, H. Wedemeyer, M. Cornberg, Treating viral hepatitis C: efficacy, side
742 effects, and complications. *Gut*. **55**, 1350–9 (2006).
743 55. E. Haasbach, K. Droebner, A. B. Vogel, O. Planz, Low-dose interferon Type I treatment is
744 effective against H5N1 and swine-origin H1N1 influenza A viruses in vitro and in vivo. *J.*
745 *Interferon Cytokine Res.* **31**, 515–25 (2011).
746 56. M. R. Loutfy, L. M. Blatt, K. A. Siminovitch, S. Ward, B. Wolff, H. Lho, D. H. Pham, H.
747 Deif, E. A. LaMere, M. Chang, K. C. Kain, G. A. Farcas, P. Ferguson, M. Latchford, G.
748 Levy, J. W. Dennis, E. K. Y. Lai, E. N. Fish, Interferon Alfacon-1 Plus Corticosteroids in
749 Severe Acute Respiratory Syndrome. *JAMA*. **290**, 3222 (2003).
750 57. M. K. Konde, D. P. Baker, F. A. Traore, M. S. Sow, A. Camara, A. A. Barry, D. Mara, A.
751 Barry, M. Cone, I. Kaba, A. A. Richard, A. H. Beavogui, S. Günther, on behalf of E. M.
752 L. European Mobile Laboratory Consortium, M. Pintilie, E. N. Fish, Interferon β-1a for
753 the treatment of Ebola virus disease: A historically controlled, single-arm proof-of-
754 concept trial. *PLoS One*. **12**, e0169255 (2017).
755 58. Q. Zhou, V. Chen, C. P. Shannon, X.-S. Wei, X. Xiang, X. Wang, Z.-H. Wang, S. J.
756 Tebbutt, T. R. Kollmann, E. N. Fish, Interferon-α2b Treatment for COVID-19. *Front.*
757 *Immunol.* **11**, 1061 (2020).
758 59. E. Davoudi-Monfared, H. Rahmani, H. Khalili, M. Hajiabdolbaghi, M. Salehi, L.
759 Abbasian, H. Kazemzadeh, M. S. Yekaninejad, Efficacy and safety of interferon β-1a in
760 treatment of severe COVID-19: A randomized clinical trial. *Antimicrob. Agents*
761 *Chemother.* (2020), doi:10.1128/AAC.01061-20.
762 60. I. F.-N. Hung, K.-C. Lung, E. Y.-K. Tso, R. Liu, T. W.-H. Chung, M.-Y. Chu, Y.-Y. Ng,
763 J. Lo, J. Chan, A. R. Tam, H.-P. Shum, V. Chan, A. K.-L. Wu, K.-M. Sin, W.-S. Leung,
764 W.-L. Law, D. C. Lung, S. Sin, P. Yeung, C. C.-Y. Yip, R. R. Zhang, A. Y.-F. Fung, E.
765 Y.-W. Yan, K.-H. Leung, J. D. Ip, A. W.-H. Chu, W.-M. Chan, A. C.-K. Ng, R. Lee, K.
766 Fung, A. Yeung, T.-C. Wu, J. W.-M. Chan, W.-W. Yan, W.-M. Chan, J. F.-W. Chan, A.
767 K.-W. Lie, O. T.-Y. Tsang, V. C.-C. Cheng, T.-L. Que, C.-S. Lau, K.-H. Chan, K. K.-W.
768 To, K.-Y. Yuen, Triple combination of interferon beta-1b, lopinavir-ritonavir, and
769 ribavirin in the treatment of patients admitted to hospital with COVID-19: an open-label,
770 randomised, phase 2 trial. *Lancet (London, England)*. **395**, 1695–1704 (2020).
771 61. D. Blanco-Melo, B. E. Nilsson-Payant, W. C. Liu, S. Uhl, D. Hoagland, R. Møller, T. X.
772 Jordan, K. Oishi, M. Panis, D. Sachs, T. T. Wang, R. E. Schwartz, J. K. Lim, R. A.
773 Albrecht, B. R. tenOever, Imbalanced Host Response to SARS-CoV-2 Drives

774 Development of COVID-19. *Cell*. **181**, 1036-1045.e9 (2020).
775 62. H. Chu, J. F.-W. Chan, Y. Wang, T. T.-T. Yuen, Y. Chai, Y. Hou, H. Shuai, D. Yang, B.
776 Hu, X. Huang, X. Zhang, J.-P. Cai, J. Zhou, S. Yuan, K.-H. Kok, K. K.-W. To, I. H.-Y.
777 Chan, A. J. Zhang, K.-Y. Sit, W.-K. Au, K.-Y. Yuen, Comparative Replication and
778 Immune Activation Profiles of SARS-CoV-2 and SARS-CoV in Human Lungs: An Ex
779 Vivo Study With Implications for the Pathogenesis of COVID-19. *Clin. Infect. Dis.*
780 (2020), doi:10.1093/cid/ciaa410.
781 63. J. Hadjadj, N. Yatim, L. Barnabei, A. Corneau, J. Boussier, N. Smith, H. Péré, B. Charbit,
782 V. Bondet, C. Chenevier-Gobeaux, P. Breillat, N. Carlier, R. Gauzit, C. Morbieu, F. Pène,
783 N. Marin, N. Roche, T.-A. Szwebel, S. H. Merkling, J.-M. Treluyer, D. Veyer, L.
784 Mouthon, C. Blanc, P.-L. Tharaux, F. Rozenberg, A. Fischer, D. Duffy, F. Rieux-Laucat,
785 S. Kernéis, B. Terrier, Impaired type I interferon activity and inflammatory responses in
786 severe COVID-19 patients. *Science* (2020), doi:10.1126/science.abc6027.
787 64. A. Vanderheiden, P. Ralfs, T. Chirkova, A. A. Upadhyay, M. G. Zimmerman, S. Bedoya,
788 H. Aoued, G. M. Tharp, K. L. Pellegrini, C. Manfredi, E. Sorscher, B. Mainou, J. E.
789 Kohlmeier, A. C. Lowen, P.-Y. Shi, V. D. Menachery, L. J. Anderson, A. Grakoui, S. E.
790 Bosinger, M. S. Suthar, Type I and Type III IFN Restrict SARS-CoV-2 Infection of
791 Human Airway Epithelial 1 Cultures 2 3 Downloaded from. *J. Virol* (2020),
792 doi:10.1128/JVI.00985-20.
793 65. K. G. Lokugamage, A. Hage, M. de Vries, A. M. Valero-Jimenez, C. Schindewolf, M.
794 Dittmann, R. Rajsbaum, V. D. Menachery, *bioRxiv*, in press,
795 doi:10.1101/2020.03.07.982264.
796 66. E. Mantlo, N. Bukreyeva, J. Maruyama, S. Paessler, C. Huang, Antiviral activities of type
797 I interferons to SARS-CoV-2 infection. *Antiviral Res.* **179**, 104811 (2020).
798 67. S. Pfaender, K. B. Mar, E. Michailidis, A. Kratzel, I. N. Boys, P. V'kovski, W. Fan, J. N.
799 Kelly, D. Hirt, N. Ebert, H. Stalder, H. Kleine-Weber, M. Hoffmann, H. Heinrich
800 Hoffmann, M. Saeed, R. Dijkman, E. Steinmann, M. Wight-Carter, M. B. McDougal, N.
801 W. Hanners, S. Pöhlmann, T. Gallagher, D. Todt, G. Zimmer, C. M. Rice, J. W.
802 Schoggins, V. Thiel, LY6E impairs coronavirus fusion and confers immune control of
803 viral disease. *Nat. Microbiol.*, 1–10 (2020).
804 68. X. Zhao, S. Zheng, D. Chen, M. Zheng, X. Li, G. Li, H. Lin, J. Chang, H. Zeng, J.-T. Guo,
805 LY6E Restricts the Entry of Human Coronaviruses, Including the Currently Pandemic
806 SARS-CoV-2. *J. Virol.* (2020), doi:10.1128/JVI.00562-20.
807 69. R. Li, H. Pei, D. K. Watson, Regulation of Ets function by protein–protein interactions.
808 *Oncogene*. **19**, 6514–6523 (2000).
809 70. A. D. Sharrocks, The ETS-domain transcription factor family. *Nat. Rev. Mol. Cell Biol.* **2**,
810 827–837 (2001).
811 71. D. Meraro, M. Gleit-Kielmanowicz, H. Hauser, B.-Z. Levi, IFN-Stimulated Gene 15 Is
812 Synergistically Activated Through Interactions Between the Myelocyte/Lymphocyte-
813 Specific Transcription Factors, PU.1, IFN Regulatory Factor-8/IFN Consensus Sequence
814 Binding Protein, and IFN Regulatory Factor-4: Characterization o. *J. Immunol.* **168**,
815 6224–6231 (2002).
816 72. T. Taniguchi, K. Ogasawara, A. Takaoka, N. Tanaka, IRF Family of Transcription Factors
817 as Regulators of Host Defense. *Annu. Rev. Immunol.* **19**, 623–655 (2001).
818 73. A. L. Brass, E. Kehrli, C. F. Eisenbeis, U. Storb, H. Singh, Pip, a lymphoid-restricted IRF,
819 contains a regulatory domain that is important for autoinhibition and ternary complex
820 formation with the Ets factor PU.1. *Genes Dev.* **10**, 2335–2347 (1996).
821 74. W. Wang, L. Xu, J. Su, M. P. Peppelenbosch, Q. Pan, Transcriptional Regulation of
822 Antiviral Interferon-Stimulated Genes. *Trends Microbiol.* **25**, 573–584 (2017).

823 75. T.-Y. Liu, T. Burke, L. P. Park, C. W. Woods, A. K. Zaas, G. S. Ginsburg, A. O. Hero, An
824 individualized predictor of health and disease using paired reference and target samples.
825 *BMC Bioinformatics*. **17**, 47 (2016).
826 76. P. C. De La Cruz-Rivera, M. Kanchwala, H. Liang, A. Kumar, L.-F. Wang, C. Xing, J. W.
827 Schoggins, The IFN Response in Bats Displays Distinctive IFN-Stimulated Gene
828 Expression Kinetics with Atypical RNASEL Induction. *J. Immunol.* **200**, 209–217 (2018).
829 77. K. Haq, J. T. Brisbin, N. Thanthrige-Don, M. Heidari, S. Sharif, Transcriptome and
830 proteome profiling of host responses to Marek's disease virus in chickens. *Vet. Immunol.*
831 *Immunopathol.* **138**, 292–302 (2010).
832 78. H. Kawagoe, M. Potter, J. Ellis, G. C. Grosveld, TEL2, an ETS factor expressed in human
833 leukemia, regulates monocytic differentiation of U937 cells and blocks the inhibitory
834 effect of TEL1 on Ras-induced cellular transformation. *Cancer Res.* **64**, 6091–6100
835 (2004).
836 79. P. Rasighaemi, A. C. Ward, ETV6 and ETV7: Siblings in hematopoiesis and its disruption
837 in disease. *Crit. Rev. Oncol. Hematol.* **116**, 106–115 (2017).
838 80. J. A. Nick, S. M. Caceres, J. E. Kret, K. R. Poch, M. Strand, A. V. Faino, D. P. Nichols,
839 M. T. Saavedra, J. L. Taylor-Cousar, M. W. Geraci, E. L. Burnham, M. B. Fessler, B. T.
840 Suratt, E. Abraham, M. Moss, K. C. Malcolm, Extremes of Interferon-Stimulated Gene
841 Expression Associate with Worse Outcomes in the Acute Respiratory Distress Syndrome.
842 *PLoS One*. **11**, e0162490 (2016).
843 81. Y. Muramoto, J. E. Shoemaker, M. Q. Le, Y. Itoh, D. Tamura, Y. Sakai-Tagawa, H. Imai,
844 R. Uraki, R. Takano, E. Kawakami, M. Ito, K. Okamoto, H. Ishigaki, H. Mimuro, C.
845 Sasakawa, Y. Matsuoka, T. Noda, S. Fukuyama, K. Ogasawara, H. Kitano, Y. Kawaoka,
846 Disease severity is associated with differential gene expression at the early and late phases
847 of infection in nonhuman primates infected with different H5N1 highly pathogenic avian
848 influenza viruses. *J. Virol.* **88**, 8981–97 (2014).
849 82. S. Davidson, M. K. Maini, A. Wack, Disease-promoting effects of type I interferons in
850 viral, bacterial, and coinfections. *J. Interferon Cytokine Res.* **35**, 252–64 (2015).
851 83. M. E. C. Meuwissen, R. Schot, S. Buta, G. Oudesluijs, S. Tinschert, S. D. Speer, Z. Li, L.
852 van Unen, D. Heijsman, T. Goldmann, M. H. Lequin, J. M. Kros, W. Stam, M. Hermann,
853 R. Willemsen, R. W. W. Brouwer, W. F. J. Van IJcken, M. Martin-Fernandez, I. de Coo,
854 J. Dudink, F. A. T. de Vries, A. Bertoli Avella, M. Prinz, Y. J. Crow, F. W. Verheijen, S.
855 Pellegrini, D. Bogunovic, G. M. S. Mancini, Human USP18 deficiency underlies type 1
856 interferonopathy leading to severe pseudo-TORCH syndrome. *J. Exp. Med.* **213**, 1163–74
857 (2016).
858 84. J.-C. Marine, D. J. Topham, C. McKay, D. Wang, E. Parganas, D. Stravopodis, A.
859 Yoshimura, J. N. Ihle, SOCS1 Deficiency Causes a Lymphocyte-Dependent Perinatal
860 Lethality. *Cell*. **98**, 609–616 (1999).
861 85. W. S. Alexander, R. Starr, J. E. Fenner, C. L. Scott, E. Handman, N. S. Sprigg, J. E.
862 Corbin, A. L. Cornish, R. Darwiche, C. M. Owczarek, T. W. . Kay, N. A. Nicola, P. J.
863 Hertzog, D. Metcalf, D. J. Hilton, SOCS1 Is a Critical Inhibitor of Interferon γ Signaling
864 and Prevents the Potentially Fatal Neonatal Actions of this Cytokine. *Cell*. **98**, 597–608
865 (1999).
866 86. B. A. Croker, D. L. Krebs, J.-G. Zhang, S. Wormald, T. A. Willson, E. G. Stanley, L.
867 Robb, C. J. Greenhalgh, I. Förster, B. E. Clausen, N. A. Nicola, D. Metcalf, D. J. Hilton,
868 A. W. Roberts, W. S. Alexander, SOCS3 negatively regulates IL-6 signaling in vivo. *Nat.*
869 *Immunol.* **4**, 540–545 (2003).
870 87. K.-P. Knobeloch, O. Utermöhlen, A. Kisser, M. Prinz, I. Horak, Reexamination of the
871 Role of Ubiquitin-Like Modifier ISG15 in the Phenotype of UBP43-Deficient Mice

Downloaded from. *Mol. Cell. Biol.* **25**, 11030–11034 (2005).

88. Y. Okada, D. Wu, G. Trynka, T. Raj, C. Terao, K. Ikari, Y. Kochi, K. Ohmura, A. Suzuki, S. Yoshida, R. R. Graham, A. Manoharan, W. Ortmann, T. Bhangale, J. C. Denny, R. J. Carroll, A. E. Eyler, J. D. Greenberg, J. M. Kremer, D. A. Pappas, L. Jiang, J. Yin, L. Ye, D.-F. Su, J. Yang, G. Xie, E. Keystone, H.-J. Westra, T. Esko, A. Metspalu, X. Zhou, N. Gupta, D. Mirel, E. A. Stahl, D. Diogo, J. Cui, K. Liao, M. H. Guo, K. Myouzen, T. Kawaguchi, M. J. H. Coenen, P. L. C. M. van Riel, M. A. F. J. van de Laar, H.-J. Guchelaar, T. W. J. Huizinga, P. Dieudé, X. Mariette, S. Louis Bridges Jr, A. Zhernakova, R. E. M. Toes, P. P. Tak, C. Miceli-Richard, S.-Y. Bang, H.-S. Lee, J. Martin, M. A. Gonzalez-Gay, L. Rodriguez-Rodriguez, S. Rantapää-Dahlqvist, L. Ärlestig, H. K. Choi, Y. Kamatani, P. Galan, M. Lathrop, S. Eyre, J. Bowes, A. Barton, N. de Vries, L. W. Moreland, L. A. Criswell, E. W. Karlson, A. Taniguchi, R. Yamada, M. Kubo, J. S. Liu, S.-C. Bae, J. Worthington, L. Padyukov, L. Klareskog, P. K. Gregersen, S. Raychaudhuri, B. E. Stranger, P. L. De Jager, L. Franke, P. M. Visscher, M. A. Brown, H. Yamanaka, T. Mimori, A. Takahashi, H. Xu, T. W. Behrens, K. A. Siminovitch, S. Momohara, F. Matsuda, K. Yamamoto, R. M. Plenge, K. Yamamoto, R. M. Plenge, Genetics of rheumatoid arthritis contributes to biology and drug discovery. *Nature*. **506**, 376–381 (2014).

89. T. James, M. Lindén, H. Morikawa, S. J. Fernandes, S. Ruhrmann, M. Huss, M. Brandi, F. Piehl, M. Jagodic, J. Tegnér, M. Khademi, T. Olsson, D. Gomez-Cabrero, I. Kockum, Impact of genetic risk loci for multiple sclerosis on expression of proximal genes in patients. *Hum. Mol. Genet.* **27**, 912–928 (2018).

90. J. E. Castañeda-Delgado, Y. Bastián-Hernandez, N. Macias-Segura, D. Santiago-Algarra, J. D. Castillo-Ortiz, A. L. Alemán-Navarro, P. Martínez-Tejada, L. Enciso-Moreno, Y. Garcia-De Lira, D. Olguín-Calderón, L. A. Trouw, C. Ramos-Remus, J. A. Enciso-Moreno, Type I Interferon Gene Response Is Increased in Early and Established Rheumatoid Arthritis and Correlates with Autoantibody Production. *Front. Immunol.* **8**, 285 (2017).

91. A. Hundeshagen, M. Hecker, B. K. Paap, C. Angerstein, O. Kandulski, C. Fatum, C. Hartmann, D. Koczan, H.-J. Thiesen, U. Klaus Zettl, Elevated type I interferon-like activity in a subset of multiple sclerosis patients: molecular basis and clinical relevance. *J. Neuroinflammation*. **9**, 574 (2012).

92. B. E. Heaton, E. M. Kennedy, R. E. Dumm, A. T. Harding, M. T. Sacco, D. Sachs, N. S. Heaton, A CRISPR Activation Screen Identifies a Pan-avian Influenza Virus Inhibitory Host Factor. *Cell Rep.* **20**, 1503–1512 (2017).

93. S. Schmid, M. Mordstein, G. Kochs, A. García-Sastre, B. R. TenOever, Transcription factor redundancy ensures induction of the antiviral state. *J. Biol. Chem.* **285**, 42013–42022 (2010).

94. N. S. Heaton, R. A. Langlois, D. Sachs, J. K. Lim, P. Palese, R. Benjamin, Long-term survival of influenza virus infected club cells drives immunopathology. **211**, 1707–1714 (2014).

95. N. C. Shaner, G. G. Lambert, A. Chammas, Y. Ni, P. J. Cranfill, M. A. Baird, B. R. Sell, J. R. Allen, R. N. Day, M. Israelsson, M. W. Davidson, J. Wang, A bright monomeric green fluorescent protein derived from Branchiostoma lanceolatum. *Nat. Methods*. **10**, 407–9 (2013).

96. J.-D. Pédelacq, S. Cabantous, T. Tran, T. C. Terwilliger, G. S. Waldo, Engineering and characterization of a superfolder green fluorescent protein. *Nat. Biotechnol.* **24**, 79–88 (2006).

97. B. S. Chambers, B. E. Heaton, K. Rausch, R. E. Dumm, J. R. Hamilton, S. Cherry, N. S.

921 Heaton, DNA mismatch repair is required for the host innate response and controls
922 cellular fate after influenza virus infection. *Nat. Microbiol.* **4**, 1964–1977 (2019).
923 98. S. M. Beaty, A. Park, S. T. Won, P. Hong, M. Lyons, F. Vigant, A. N. Freiberg, B. R.
924 tenOever, W. P. Duprex, B. Lee, Efficient and Robust Paramyxoviridae Reverse Genetics
925 Systems. *mSphere*. **2** (2017), doi:10.1128/mSphere.00376-16.
926 99. C. T. Workman, Y. Yin, D. L. Corcoran, T. Ideker, G. D. Stormo, P. V. Benos,
927 enoLOGOS: a versatile web tool for energy normalized sequence logos. *Nucleic Acids*
928 *Res.* **33**, W389–W392 (2005).
929 100. S. Babicki, D. Arndt, A. Marcu, Y. Liang, J. R. Grant, A. Maciejewski, D. S. Wishart,
930 Heatmapper: web-enabled heat mapping for all. *Nucleic Acids Res.* **44**, W147–W153
931 (2016).
932 101. H. A. R. Bluyssen, R. J. Vlietstra, P. W. Faber, E. M. E. Smit, A. Hagemeijer, J. Trapman,
933 Structure, Chromosome Localization, and Regulation of Expression of the Interferon-
934 Regulated Mouse Ifi54/Ifi56 Gene Family. *Genomics*. **24**, 137–148 (1994).
935 102. T. Ohtomo, Y. Sugamata, Y. Ozaki, K. Ono, Y. Yoshimura, S. Kawai, Y. Koishihara, S.
936 Ozaki, M. Kosaka, T. Hirano, M. Tsuchiya, Molecular Cloning and Characterization of a
937 Surface Antigen Preferentially Overexpressed on Multiple Myeloma Cells. *Biochem.*
938 *Biophys. Res. Commun.* **258**, 583–591 (1999).
939 103. W. Yang, J. Tan, R. Liu, X. Cui, Q. Ma, Y. Geng, W. Qiao, Interferon-γ Upregulates
940 Expression of IFP35 Gene in HeLa Cells via Interferon Regulatory Factor-1. *PLoS One*. **7**
941 (2012), doi:10.1371/JOURNAL.PONE.0050932.
942 104. M. G. Wathelet, C. H. Lin, B. S. Parekh, L. V Ronco, P. M. Howley, T. Maniatis, Virus
943 infection induces the assembly of coordinately activated transcription factors on the IFN-
944 beta enhancer in vivo. *Mol. Cell*. **1**, 507–18 (1998).
945 105. B. Testoni, V. Schinzari, F. Guerrieri, S. Gerbal-Chaloin, G. Blandino, M. Levrero, p53-
946 paralog DNp73 oncogene is repressed by IFNα/STAT2 through the recruitment of the
947 Ezh2 polycomb group transcriptional repressor. *Oncogene*. **30**, 2670–8 (2011).
948 106. M. N. Rutherford, G. E. Hannigan, B. R. Williams, Interferon-induced binding of nuclear
949 factors to promoter elements of the 2-5A synthetase gene. *EMBO J.* **7**, 751–9 (1988).
950 107. Q. Wang, G. Floyd-Smith, The p69/71 2-5A synthetase promoter contains multiple
951 regulatory elements required for interferon-α-induced expression. *DNA Cell Biol.* **16**,
952 1385–1394 (1997).
953 108. D. Rebouillat, A. Hovnanian, G. David, A. G. Hovanessian, B. R. G. Williams,
954 Characterization of the Gene Encoding the 100-kDa Form of Human 2′,5′Oligoadenylate
955 Synthetase. *Genomics*. **70**, 232–240 (2000).
956 109. N. Wang, Q. Dong, J. Li, R. K. Jangra, M. Fan, A. R. Brasier, S. M. Lemon, L. M. Pfeffer,
957 K. Li, Viral induction of the zinc finger antiviral protein is IRF3-dependent but NF-
958 kappaB-independent. *J. Biol. Chem.* **285**, 6080–90 (2010).
959
960

961 **Acknowledgements:** We acknowledge assistance from Mike Cook and the Duke Cancer Institute
962 Flow Cytometry Core. We thank Robert Lefkowitz and his laboratory for assistance with and use
963 of the ChemiDoc Imaging System. We would like to thank Dr. Clare Smith for help establishing
964 SARS-CoV-2 viral infection assays at BSL3. We also thank Ephraim Tsalik, Micah McClain, and
965 Bandita Gershon for helpful discussions and Ben Chambers, Stacy Webb, and other members of
966 the Heaton lab for critical reading of the manuscript. **Funding:** Biocontainment work was
967 performed in the Duke Regional Biocontainment Laboratory under the direction of Greg
968 Sempowski, which received partial support for construction from the National Institutes of Health,
969 National Institute of Allergy and Infectious Diseases (UC6-AI058607). H.M.F. and A.T.H. were
970 supported by NIH training grant T32-CA009111. N.S.H. is supported by R01-HL142985, R01-
971 AI137031, and funding from the Defense Advanced Research Projects Agency's (DARPA)
972 PReemptive Expression of Protective Alleles and Response Elements (PREPARE) program
973 (Cooperative agreement #HR00111920008). The views, opinions and/or findings expressed are
974 those of the author and should not be interpreted as representing the official views or policies of
975 the U.S. Government. **Author contributions:** H.M.F., A.T.H. and N.S.H. designed the study.
976 H.M.F., A.T.H., and B.E.H. performed experiments. H.M.F., A.T.H. and N.S.H. analyzed data.
977 H.M.F. and N.S.H. wrote the paper. **Competing interests:** The authors declare no competing
978 interests. **Data and materials availability:** All next generation sequencing data are available at
979 NCBI GEO under accession number GSE140718. The following reagent was deposited by the
980 Centers for Disease Control and Prevention and obtained through BEI Resources, NIAID, NIH:
981 SARS-Related Coronavirus 2, Isolate USA-WA1/2020, NR-52281.
982
983
984